

# Targeting Ubiquitin-Specific Protease 7 with Novel 5-Amino-Pyrazole Inhibitors: Design, Synthesis, and Biological Evaluation

Matteo Lusardi, Elva Morretta, Andrea Spallarossa, Maria Chiara Monti, Camillo Rosano, Erika Iervasi, Marco Ponassi, Matteo Mori, Fiorella Meneghetti, and Chiara Brullo\*

To further extend the structure–activity relationships (SARs) of the previously published ubiquitin-specific protease 7 (USP-7) inhibitor **STIRUR-41**, a small library of 5-aminopyrazoles **1a–d** and **2a–d** is designed and synthesized. The chemical identity of the desired structure is confirmed by nuclear magnetic resonance and single crystal X-ray diffraction analyses. All novel derivatives are tested as potential USP-7 inhibitors and compounds **1a–d** block enzyme activity in a dose-dependent manner and with lower IC<sub>50</sub> values compared to the lead compound **STIRUR-41**. Notably, **1d**, bearing

a *meta*-trifluoromethylphenyl group linked to the carbamate moiety, proved to be the most active candidate. Conversely, compounds belonging to series **2**, which possess greater steric hindrance, exhibit no activity. The most effective compounds of series **1** are noncytotoxic across a panel of tumor and normal cell lines at 10 μM concentration. For the most active compound **1d**, a parallel artificial membrane permeability assay is also performed, as well as docking and molecular dynamics simulations.

## 1. Introduction

The ubiquitin–proteasome system is the main protein regulatory system present in all eukaryotic cells, allowing the regulation, and consequently, elimination of all misfolded, aggregated, or unnecessary proteins, thus maintaining cellular homeostasis.<sup>[1]</sup>

Protein ubiquitination is a post-translational dynamics and reversible process that can be reversed by deubiquitinating

enzymes (**Figure 1**), called deubiquitinases (DUBs). Out of the seven DBU families, the ubiquitin-specific protease 7 (USP-7) family (also known as herpesvirus-associated ubiquitin-specific protease) is the largest.<sup>[2]</sup> In the human genome, the USP-7 family consists of 58 members that regulate many cellular proteins, including those involved in viral replication, immune response, epigenetic control, apoptosis, DNA damage response, and DNA replication and transcription. The role of USP-7 in regulating these cellular pathways suggested this enzyme as a novel promising therapeutic target for oncology therapy.<sup>[3,4]</sup> Notably, elevated USP-7 activity has been correlated with the onset, and subsequent progression of various human tumors through the interaction with oncogenic proteins, such as MDM2, MDMX,<sup>[5]</sup> β-catenin,<sup>[6]</sup> NF-κB,<sup>[7]</sup> FOXp3,<sup>[8]</sup> tumor suppressors p53, and PTEN.<sup>[9]</sup> Furthermore, USP-7 activity is also involved in cancer angiogenesis, facilitating the formation of new blood vessels within the tumor microenvironment.<sup>[10]</sup> However, its role in tumor pathologies is dual, acting both as a promoter and as a tumor suppressor, depending on the cancer type.<sup>[11,12]</sup> In detail, USP-7 overexpression has been observed in numerous malignant tumors, where it serves as a predictive marker of cancer progression and poor prognosis. In contrast, USP-7 low expression has been identified in some neuroendocrine lung tumors<sup>[13]</sup> and in nonsmall cell lung adenocarcinoma,<sup>[14]</sup> suggesting that the role of USP-7 can vary across different cancer types and may differently influence tumor behavior.

For all these reasons, in the last years, USP-7 has emerged as a novel and exciting therapeutic target for cancer treatment, and several covalent and noncovalent small-molecule inhibitors have been developed with promising efficacy in preclinical studies.<sup>[15–23]</sup> Particularly, monocycles (e.g., thiazoles and pyridines) or bicyclic (e.g., quinazolines, pyrazolo-pyrimidines, thieno-pyrimidines, and


M. Lusardi, A. Spallarossa, C. Brullo  
 Department of Pharmacy  
 Università degli Studi di Genova  
 viale Benedetto XV, 3, 16132 Genova, Italy  
 E-mail: chiara.brullo@unige.it


M. Lusardi  
 Molecular Modeling and Drug Discovery Laboratory  
 Istituto Italiano di Tecnologia  
 Via Morego, 30, 16163 Genova, Italy

E. Morretta, M. Chiara Monti  
 Department of Pharmacy  
 University of Naples “Federico II”  
 Via Domenico Montesano, 49, 80131 Napoli, Italy

C. Rosano, E. Iervasi, M. Ponassi  
 Proteomics and Mass Spectrometry Laboratory  
 IRCCS Ospedale Policlinico San Martino  
 L.go. R. Benzi, 10 I, 16132 Genova, Italy

M. Mori, F. Meneghetti  
 Department of Pharmaceutical Sciences  
 University of Milan  
 Via L. Mangiagalli, 25, 20133 Milano, Italy

 Supporting information for this article is available on the WWW under <https://doi.org/10.1002/cmdc.202500185>

 © 2025 The Authors. ChemMedChem published by Wiley-VCH GmbH. This is an open access article under the terms of the Creative Commons Attribution License, which permits use, distribution and reproduction in any medium, provided the original work is properly cited.

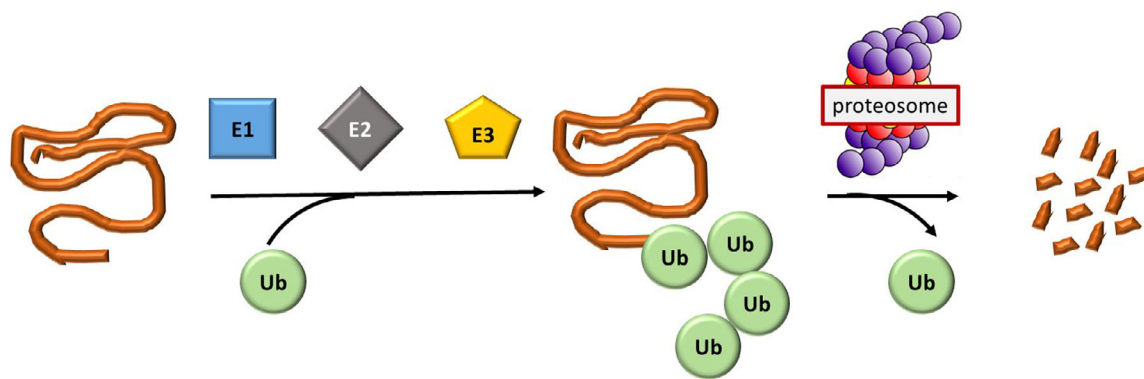


**Figure 1.** Schematic representation of the ubiquitin–proteasome system. Ub = ubiquitin. E1 = E1 ligase. E2 = E2 ligase. E3 = E3 ligase.

imidazo-triazines) and tricyclic derivatives (e.g., triterpenoid derivatives) have been recently published and patented.<sup>[16]</sup>

In this context, our previous investigations led to the identification of a large library of pyrazole derivatives able to block IL-8-induced chemotaxis of human neutrophils.<sup>[24]</sup> In detail, the most active compound **STIRUR-41** (Figure 2) was submitted for additional investigations, showing a significant inhibition of migratory ability of neuroblastoma HTLA-230 cells.<sup>[25]</sup> Subsequent, drug affinity-responsive target stability studies coupled to limited proteolysis-coupled mass spectrometry, along with in vitro and in-cell assays, recently demonstrated the ability of **STIRUR-41** to inhibit both the enzymatic activity of USP-7 and its expression levels in neuroblastoma-related cells.<sup>[26]</sup>

To further extend the structure–activity relationship (SAR) of **STIRUR-41**, the first-in-class pyrazole-based USP-7 inhibitor, 5-aminopyrazoles (5APs) **1** and **2** (Figure 2) were designed and synthesized. Specifically, the phenylaminocarbonyl portion was formally shifted from the 5-nitrogen atom of **STIRUR-41** to the oxygen atom of the side chain, leading to the carbamate analogs **1** and **2**. The structure of the novel compounds was fine-tuned by inserting fluorinated substituents (namely, F and CF<sub>3</sub>, selected on the basis of previously defined SARs) at different positions of the carbamate-bound phenyl ring and by modifying the length of the side chain (i.e., 2-hydroxypropyl and 2-hydroxybutyl moieties).

We confirmed the formation of the desired structures by nuclear magnetic resonance (NMR) and X-ray crystallographic analysis. Then, all newly synthesized compounds were evaluated for their in vitro USP-7 inhibition. The most active compounds were also evaluated for their cytotoxicity (MTT

assays at 10 μM concentration) in several cancer cell lines as well as in healthy human embryonic fibroblasts (GM-6114) to verify that they did not affect cell viability, as the previous lead **STIRUR-41**. Moreover, pharmacokinetics and toxicity properties as well as their drug-likeness [SwissADME and ProTox web server] were calculated. Finally, parallel artificial membrane permeability assay (PAMPA) analysis was performed as well as docking and molecular dynamics simulations.

## 2. Results and Discussion

### 2.1. Chemistry

Compounds **1** and **2** were obtained starting from the 5-aminopyrazole intermediates **3a,b**, synthesized as previously reported (Scheme 1).<sup>[24]</sup> Briefly, the condensation of **3a** with the properly substituted isocyanate in anhydrous DMF at 100 °C for 12 h led to the isolation of compounds **1a–d** in moderate yields (23%–53%). Unfortunately, under these reaction conditions, 5-aminopyrazole **3b** proved to be unreactive toward isocyanates, possibly due to the increase of the steric hindrance of the ethyl group adjacent to the alcohol functionality. Therefore, compounds **2a–d** were obtained through an alternative synthetic procedure involving the use of anhydrous toluene as a solvent, an excess of isocyanate reagent (3 equivalents), and two cycles of microwave heating (300 W, 7 min). With both methods, the final compounds were isolated through column chromatography (silica gel) using dichloromethane and ethyl ether as eluents.

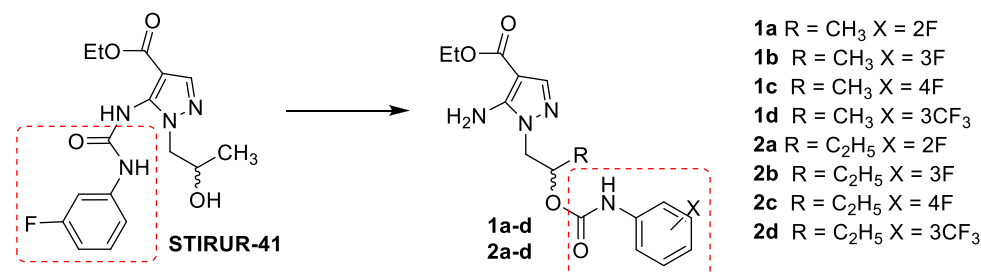
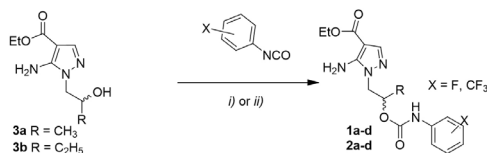


**Figure 2.** Molecular structure of the lead compound **STIRUR-41** and the new 5-amino carbamoyl derivatives **1a–d** and **2a–d**.



**Scheme 1.** Synthesis of the new compounds **1a–d** and **2a–d**. i) Proper phenyl isocyanate, an. DMF, 100 °C, 12 h (yield: 23%–43%) and ii) excess of proper phenyl isocyanate, an. toluene, microwave, 100 °C, 300 W, 2 × 7 min (yield: 16%–27%).

Interestingly, pyrazoles **3** bear two nucleophilic centers (i.e., the NH<sub>2</sub> and OH groups) potentially able to react with the isocyanate reagents. However, the different reaction conditions were found to affect the regioselectivity of the condensation. In detail, as previously reported, the use of an apolar solvent (toluene) under conventional heating conditions oriented the reaction toward the amino group of **3**, leading to the isolation of urea derivatives.<sup>[24,27]</sup> Conversely, heating the toluene mixture under microwave irradiation with an excess of heterocumulene or using polar aprotic solvents (e.g., DMF) led to the preferential reaction of the alcohol functionality allowing the formation of carbamate compounds.<sup>[28]</sup>

The chemical identity of compounds **1** and **2** was determined by both NMR and X-ray crystallography analyses. Specifically, the proton NMR signals at 6.00 ppm (present also in the spectra of precursors **3**) and the lack of the signal at 4.93 ppm (assigned to the OH in the spectra of **3**) indicated the presence of the free amino group at position 5 and confirmed the functionalization of the hydroxyl group in derivatives **1** and **2** (Figure 3).

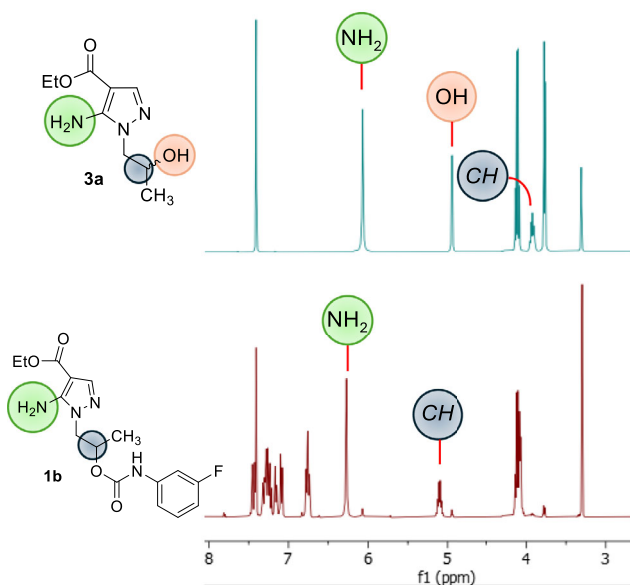


**Figure 3.** Comparison of the <sup>1</sup>H NMR spectra of derivatives **3a** and **1b**. Relevant signals are highlighted.

## 2.2. X SC-XRD Study of **1b**

The structure of **1b** was investigated by single crystal X-ray diffraction (SC-XRD) to confirm the success of the functionalization of the hydroxyl group and study the 3D features of this new class of 5-APs. The compound crystallized in the orthorhombic system, with space group Pca2<sub>1</sub>. Its thermal ellipsoid diagram is shown in Figure 4.

The asymmetric unit (ASU) contains two independent molecules, which overlay with a low root mean square deviation (RMSD) (0.1339 Å). The largest deviation (0.474 Å) occurs at the terminal methyl (C16) of the ethyl ester, reflecting minor structural flexibility. The analysis suggests a degree of pseudosymmetry, as the overall molecular arrangement nearly conforms to a higher-symmetry space group, though the crystal ultimately refines in the noncentrosymmetric space group Pca2<sub>1</sub>. The compound contains a chiral center at C5/C5A. However, the Flack parameter converges to a meaningless value of −0.2(7) using Parsons' method, likely due to a combination of factors, including the absence of anomalous scatterers and the pseudosymmetry, which increase the instability and uncertainty of the parameter. Therefore, despite this deviation from the ideal value, the molecule appears to be a racemate. The compound consists of two nearly parallel planar regions, corresponding to the substituted aminopyrazole and the phenyl carbamate moieties. These regions are connected by a methylene and a methine carbon atoms, forming dihedral angles of −164.4(3)° for N1–C4–C5–O1 and −164.9(3)° for N1A–C4A–C5A–O1A. The largest deviations from the mean planes calculated for the pyrazole and phenyl ring are observed in the ethyl ester, specifically at C16 (0.43 Å) and C15A (0.23 Å), and in the carbamate's alkoxy oxygen, at O1 (0.23 Å) and O1A (0.20 Å), respectively. The two planes are inclined at 8.4° and 10.7° with respect to each other in the number-labeled and letter-labeled molecules of the ASU, respectively.

The structure is characterized by strong intramolecular H-bonds, connecting the amino group (N4, N4A) to the two carbonyl oxygens (O2 and O3, O2A and O3A) of the carbamate and ester moieties (Figure 5A). These interactions play a key role in defining the molecular conformation, leading to atypical angles and torsions, as confirmed by the CSD Mogul analysis. Specifically, the previously mentioned dihedral angles deviate significantly from the typical range (45°–90°). Likewise, the C4–N1–C3 (126.5(3)°) and C4A–N1A–C3A (126.4(3)°) angles are notably smaller than the average value observed in similar structures (130.534°). The intermolecular network is also largely governed by H-bonds. The main one connects the carbamate NH (N3/N3A) to one of the nitrogen atoms (N2/N2A) of the pyrazole ring of an adjacent molecule. Additional weaker interactions are formed between the aromatic CH groups and the N, O, and F atoms of nearby molecules. A complete account of H-bonds is provided in Table 1.  $\pi$ - $\pi$  Stacking contributes marginally to the crystal packing, with an inclined interaction between the phenyl groups, characterized by a centroid–centroid distance of 4.46 Å. Overall, the spatial organization of the crystal follows a double offset zig-zag pattern (Figure 5B).

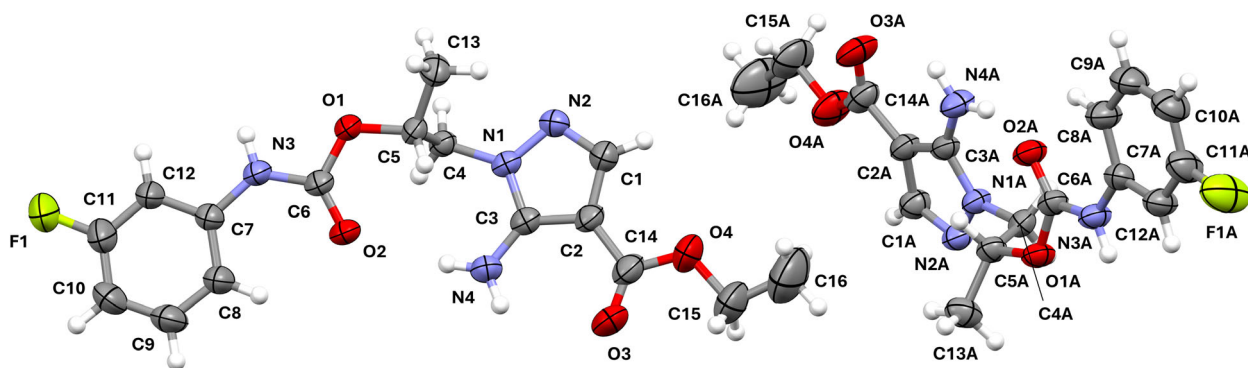


Figure 4. Thermal ellipsoid diagram of **1b**, with the arbitrary atom-numbering scheme. Displacement ellipsoids are drawn at the 40% probability level.

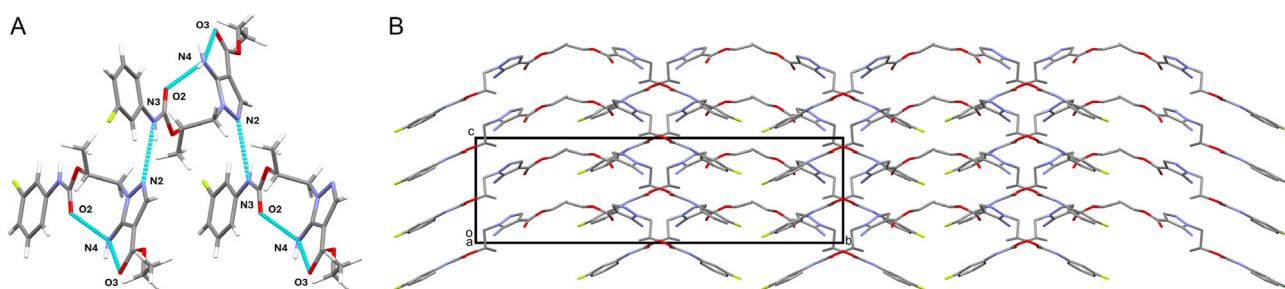
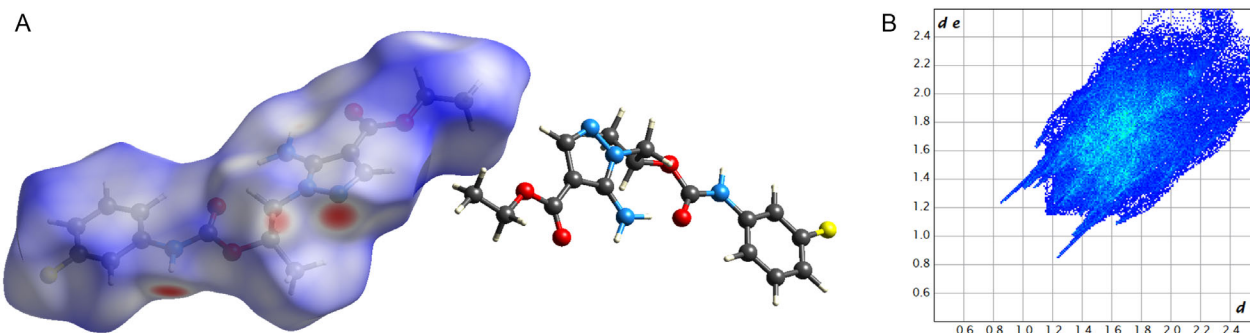


Figure 5. A) Stick model of **1b** showing the main H-bonds as cyan dotted lines. B) Stick model showing the crystal packing of **1b**, viewed along the *a* axis. For the sake of clarity, hydrogen atoms are omitted.

Table 1. H-bond geometry (D: donor, a: acceptor) for <b>1b</b> .					
	D-H/Å	H...A/Å	D...A/Å	D-H...A/°	Equivalent positions
N4—H4W...O2 <sup>i</sup>	0.860(3)	2.422(3)	3.210(4)	152.7(2)	<sup>i</sup> <i>x, y, z</i> ; <sup>ii</sup> <i>1-x, 2-y, z-1/2</i> ; <sup>iii</sup> <i>2-x, 1-y, z-1/2</i> ; <sup>iv</sup> <i>x-1/2, 1-y, z</i> ; <sup>v</sup> <i>1-x, 1-y, z-1/2</i> ; <sup>vi</sup> <i>x, y+1, z</i> ; <sup>vii</sup> <i>2-x, 2-y, z-1/2</i> ; <sup>viii</sup> <i>x, y-1, z</i>
N4—H4X...O3 <sup>i</sup>	0.860(3)	2.428(4)	2.957(5)	120.3(2)	
N4A—H4Y...O2A <sup>i</sup>	0.860(3)	2.451(3)	3.250(4)	154.8(3)	
N4A—H4Z...O3A <sup>i</sup>	0.860(3)	2.440(4)	2.969(5)	120.4(3)	
C8—H8...O2 <sup>i</sup>	0.930(4)	2.310(3)	2.911(5)	121.9(3)	
C8A—H8A...O2A <sup>i</sup>	0.930(5)	2.335(3)	2.931(6)	121.6(3)	
N3A—H3A...N2A <sup>ii</sup>	0.860(3)	2.181(3)	3.023(4)	166.2(2)	
C12A—H12A...N2A <sup>ii</sup>	0.930(4)	2.844(3)	3.582(5)	137.2(3)	
C12—H12...N2 <sup>iii</sup>	0.930(4)	2.834(3)	3.567(5)	136.5(3)	
N3—H3...N2 <sup>iii</sup>	0.860(3)	2.248(3)	3.070(4)	160.0(2)	
N4—H4X...O1 <sup>iv</sup>	0.860(3)	2.939(3)	3.615(4)	136.9(2)	
C9—H9...O3 <sup>v</sup>	0.930(5)	2.517(3)	3.431(6)	167.7(3)	
C10A—H10A...F1A <sup>vi</sup>	0.930(5)	2.655(4)	3.368(6)	134.1(3)	
C9A—H9A...O3A <sup>vii</sup>	0.930(5)	2.466(3)	3.385(6)	169.8(3)	
C10—H10...F1A <sup>viii</sup>	0.930(6)	2.586(3)	3.499(6)	167.0(3)	

The Hirshfeld surface (HS) was computed for both molecules in the ASU, revealing similar features (HS-1, V: 439.72 Å<sup>3</sup>, A: 399.52 Å<sup>2</sup>, G: 0.700, Ω: 0.440; HS-A, V: 437.58 Å<sup>3</sup>, A: 401.30 Å<sup>2</sup>, G: 0.695, Ω: 0.458). The HS mapped over the  $d_{norm}$  property exhibits several red spots, both intense and faint, corresponding to the numerous traditional and nontraditional

( $\pi$ H...N/O/F) H-bonds established within the crystal structure (Figure 6A). The 2D fingerprint plot has a compact and slightly elongated shape, with two spikes protruding toward the lower left part of the graph (short-range region), at  $d_e/d_i$  values compatible with NH...N bonds (Figure 6B). Shorter spikes, partially superposed to the previous ones, represent contact between



**Figure 6.** A) HS-1 of **1b** mapped over  $d_{norm}$  with a fixed color scale in the range  $-0.4051$  au (red)– $1.6347$  au (blue). Red, blue, and white indicate intermolecular contacts shorter, longer, and approximately equal to the sum of their van der Waals radii, respectively. B) 2D Fingerprint plot of **1b**. Each point represents a unique  $d_e/d_i$  pair, and its color indicates its contribution to the surface area: blue for low contribution, green for moderate, and red for high. Uncolored points have no contribution.

aromatic hydrogens and heteroatoms (N/O/F). The plot also shows the presence of some stacking interactions (C–C contacts), although their contribution is marginal with respect to that of H-bonds. The enrichment ratios confirm that N...H/H...N, O...H/H...O, F...H/H...F, and C...C contacts are favored, further corroborating the analysis of the intermolecular network (Table S1, Supporting Information).

### 2.3. Evaluation of Compound Effect on USP-7 Enzymatic Activity

The inhibition efficiency of compounds **1a–d** and **2a–d** on the USP-7 enzyme was assessed using a fluorescence-based enzymatic assay, employing Ubiquitin–AMC as a substrate. In this assay, USP-7 hydrolyzes Ubiquitin–AMC, leading to an increase in fluorescence signal. To evaluate the inhibitory potential, recombinant USP-7 was preincubated with varying concentrations of the test compounds before adding the substrate, and fluorescence intensity was subsequently measured. The results revealed that compounds **1a–d** caused a reduction in fluorescence intensity, conceivably related to USP-7 inhibition, in a dose-dependent manner and with lower  $IC_{50}$  values compared to the lead compound **STIRUR-41** (Table 2 and Figure S1, Supporting Information). Compound **1d**, characterized by a *meta*-trifluoromethylphenyl group linked to the carbamate moiety, was the most active, while **1a**, which carries an *ortho*-fluorine atom, proved to be the least potent. Additionally, the elongation of the side chain in compounds **2a–d** completely abolished the activity.

**Table 2.**  $IC_{50}$  values of compounds **1a–d** and **STIRUR-41** (used as reference compound) against recombinant USP-7. The reported values are the average of three separate experiments.

Cpd	$IC_{50}$ [ $\mu$ M] $\pm$ SD	$R^2$
<b>1a</b>	$2.19 \pm 0.49$	0.873
<b>1b</b>	$1.48 \pm 0.31$	0.889
<b>1c</b>	$1.80 \pm 0.39$	0.879
<b>1d</b>	$1.31 \pm 0.21$	0.932
<b>STIRUR-41</b>	$2.77 \pm 0.56$	0.947

### 2.4. Cytotoxicity

To evaluate the cytotoxicity of the novel USP-7 inhibitors, compounds **1a–d** were preliminary screened at a fixed concentration of  $10 \mu$ M against eight different cancer cell lines (namely, MCF7 breast adenocarcinoma, SKOV-3 ovarian adenocarcinoma, Hep-G2 hepatocellular carcinoma, SK-Mel28 cutaneous melanoma, MDA-MB-231 breast adenocarcinoma, SK-BR3 breast adenocarcinoma, HeLa cervix epithelioid carcinoma, and A549 lung adenocarcinoma) as well as nonmutated human embryonic fibroblasts (GM-6114). Cisplatinium (*Cis*-Pt) was used as the reference compound. As reported in Table 3, compounds from series **1** were noncytotoxic across all tested cell lines (survival percentage values greater than 68%), with the unique exception of compound **1b**, which showed moderate cytotoxicity only against A549 cells (survival percentage = 39%). Collectively, **STIRUR-41** and novel compounds **1a–d** showed a very similar antiproliferative profile, and interestingly, **STIRUR-41** evidenced a major toxicity on healthy GM-6114 cell lines. Consequently, we can hypothesize a better pharmacological profile of most active derivative **1d** respect to our lead **STIRUR-41**.

### 2.5. Pharmacokinetic Properties, Drug-Likeness, and Toxicity Prediction

The pharmaceutical, pharmacokinetic, and drug-likeness properties of the most active compound **1d** and the lead **STIRUR-41** were calculated by SwissADME.<sup>[29]</sup> In the simulation, the two derivatives showed similar drug-likeness and pharmacokinetic properties (Table S3, Supporting Information). Specifically, the fraction  $Csp^3$  was 0.35 and 0.31, the Log P (XLOGP3) values were 3.18 and 1.68, the number of rotatable bonds was 10 and 9, the number of H-bond acceptors was 8 and 6, the number of H-bond donors was 2 and 3, and the topological polar surface area was 108.47 and 105.48  $\text{\AA}^2$ , for **1d** and **STIRUR-41**, respectively. Altogether these compounds were predicted to be water soluble, characterized by high gastrointestinal absorption, and unable to cross the blood brain barrier. Differently to **STIRUR-41**, **1d** was not flagged as a substrate for Pgp. In addition, no violations of the Lipinski rules were detected.

Finally, the toxicity profiles of **1d** and **STIRUR-41** were predicted using ProTox webserver.<sup>[30]</sup> According to the simulation, the

**Table 3.** Cell growth percent values for compounds **1a-d** and Cis-Pt (reference) on different cancer cell lines at 10  $\mu\text{M}$  concentration. Data are mean values of three separate experiments. Variation among triplicate samples is less than 10%.

Tumor cell line	Cell growth percent [%]					
	1a	1b	1c	1d	STIRUR-41	Cis-Pt
<b>Lung adenocarcinoma</b>						
A549	104.43	39.06	114.96	90.69	38.88	59.09
<b>Cervix epithelioid carcinoma</b>						
HeLa	105.06	95.63	108.28	106.40	99.83	29.33
<b>Hepatocellular carcinoma</b>						
Hep-G2	97.50	95.70	100.11	100.73	111.36	38.07
<b>Breast cancer</b>						
MCF7	109.46	104.08	108.02	113.85	110.71	72.74
MDA-MB-231	106.29	73.53	103.39	119.94	64.32	86.07
SK-BR3	98.76	135.91	101.55	95.04	97.17	70.59
<b>Cutaneous melanoma</b>						
SK-Mel28	95.28	115.09	88.22	90.77	94.26	44.40
<b>Ovarian adenocarcinoma</b>						
SKOV-3	102.26	98.78	99.94	99.40	100.50	26.83
<b>Human embryonic fibroblasts</b>						
GM-6114	105.96	68.07	112.09	96.18	38.50	39.52

predicted  $\text{LD}_{50}$  values for **STIRUR-41** and **1d** were 1000 and 1550  $\text{mg Kg}^{-1}$ , respectively, being classified in the toxicity class 4. Interestingly, **1d** may only induce neurotoxicity, potentially emerging as a less toxic analog of **STIRUR-41**, which is characterized by predicted neurotoxicity, nephrotoxicity, and respiratory toxicity.

## 2.6. PAMPA Assay

The membrane permeability of the most active derivative **1d** was determined using the PAMPA at two different concentrations (100 and 250  $\mu\text{M}$ , respectively). Propranolol and furosemide were included as reference compounds for high and low permeability, respectively. The compound proved to be highly permeable at the tested concentrations, showing  $\text{Log } P_e$  values comparable to those of propranolol (Table 4).

## 2.7. Docking Simulations

To further characterize the interaction between **1d** and USP-7, docking simulations (Autodock4.2)<sup>[31]</sup> were carried out on the USP-7N-terminal domain (PDB code: 5N9T).<sup>[32]</sup> The docking protocol was validated through a redocking procedure on the cocrystallized ligand (RMSD value over heavy atoms = 0.474 Å;

**Table 4.**  $\text{Log } P_e$  values of **1d**. Data are mean values of three separate experiments.

Sample (concentration)	$\text{Log } P_e \pm \text{SD}$
Propranolol (250 $\mu\text{M}$ )	$-4.61 \pm 0.01$
Furosemide (250 $\mu\text{M}$ )	$-5.29 \pm 0.02$
<b>1d</b> (100 $\mu\text{M}$ )	$-4.54 \pm 0.02$
<b>1d</b> (250 $\mu\text{M}$ )	$-4.81 \pm 0.00$

RMSD value over all atoms = 0.855 Å). Both enantiomers of the most active compound of the series were considered. In the USP-7/(**R**)-**1d** docking complex (calculated  $K_i = 2.85 \mu\text{M}$ ; estimated free energy of binding =  $-7.56 \text{ kcal mol}^{-1}$ ), the ligand would assume an extended conformation with the carbamate portion pointing toward the bulk solvent and the pyrazole moiety inserted into the binding site (Figure 7).

The complex would be mainly stabilized by two hydrogen bonds, involving 1) the carbamate NH atom and Asp295 side chain and 2) the ester carbonyl and His461 side chain. Further, stabilization would be provided by Van Der Waals interactions between: 1) the pyrazole core and Tyr224 and Val296, 2) the carbon side chain and Asp295, Val296, Gln297, and Gln405, and 3) the 3- $\text{CF}_3$ -phenyl portion, and Phe409 and Asn418.

In the USP-7/(**S**)-**1d** docking complex, the ligand would adopt a similar bioactive conformation to that calculated for the (**R**)-enantiomer. However, the different stereochemistry would affect the orientation of the pyrazole substructure, preventing the formation of the hydrogen bond between the ester functionality and His461. Despite the lack of this relevant interaction, the calculated  $K_i$  value of the USP-7/(**S**)-**1d** complex is slightly lower than that predicted for the USP-7/(**R**)-**1d** complex (calculated  $K_i = 2.51 \mu\text{M}$ ; estimated free energy of binding =  $-7.64 \text{ kcal mol}^{-1}$ ), thus, indicating that the (**S**) enantiomer should represent the eutomer.

## 2.8. Molecular Dynamics Simulations

To further assess the reliability of the docking calculations, a molecular dynamics simulation (NAMD software, explicit solvent,  $T = 310 \text{ K}$ , time = 10 ns) was carried out on the USP-7/(**S**)-**1d** model, selected as the most promising docking complex. The molecular dynamics trajectory highlighted a stable binding

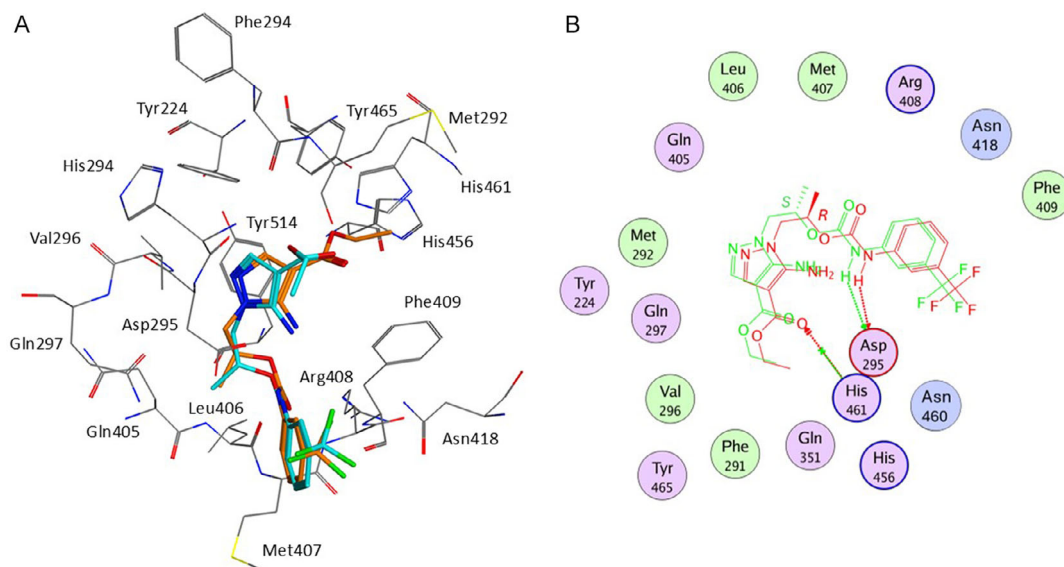


**Figure 7.** A) Docking poses of **1d(R)** (cyan) and **1d(S)** (orange) in USP-7 binding site. B) Superposition of the log plot for the USP-7/**1d(R)** and USP-7/**1d(S)** complexes.

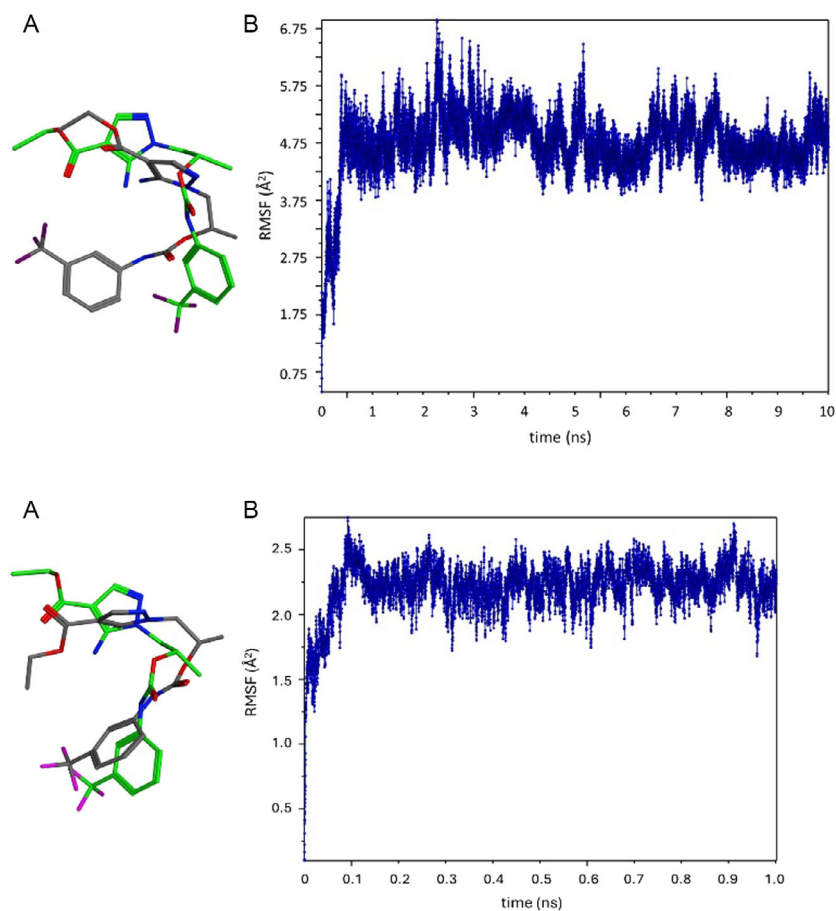


**Figure 8.** A) Superposition of the initial (green) and final (gray) bioactive conformation of **(S)-1d**. B) Time-dependent root-mean-square fluctuation analysis of ligand **(S)-1d**.

between the ligand and the protein, with minimal fluctuations from the docking pose (Figure 8). Furthermore, the analysis of the hydrogen bond network between (S)-1d and USP-7 residues indicated that the ligand could form one to three H-bonds with the protein. In particular, the interaction between the carbamate NH or NH<sub>2</sub> groups and Asp295 side chain would be the most likely H-bond, being observed in the 16.54% of the MD conformations. Additional H-bonds would involve the ligand and Arg408 main chain and carbamic carbonyl (frequency = 9.31%), Gln351 side chain and pyrazole nitrogen (frequency = 2.88%), and Tyr465 phenol group and ester carbonyl (frequency = 1.06%). Other amino acids H-bonded to (S)-1d would include Phe409 (0.33%), Leu406 (0.29%), Asn418 (0.26%), Tyr411 (0.19%), Val296 (0.06%), His461 (0.06%), and Gln297 (0.06%).

### 3. Conclusions

Collectively, the newly synthesized 5-aminopyrazoles (SAPs) 1a–d, featuring a carbamate function on the N1 alkyl chain, demonstrated potent and dose-dependent inhibition of USP-7, achieving lower IC<sub>50</sub> values than the lead compound STIRUR-41. In contrast, compounds from series 2, which possess greater steric hindrance, were completely inactive, highlighting the importance, as key element for an effective enzyme binding, of the structural flexibility.

The enzymatic data strongly support the role of specific structural modifications in enhancing USP-7 inhibition. While a bulkier N1 alkyl chain negatively affects activity, the introduction of halogen atoms (especially fluorine) at different positions of the carbamate-linked aromatic ring positively influences biological potency.

Collectively, the pyrazole derivatives reported here showed similar potency to other recently described monocyclic inhibitors (percentage of inhibition in the low micromolar range).<sup>[16]</sup> Particularly, among the tested derivatives, compound 1d emerged as the most promising, exhibiting strong USP-7 inhibition and high membrane permeability (as confirmed by PAMPA). In addition, respect to the lead STIRUR-41, 1d showed lesser toxicity on healthy human embryonic fibroblasts GM-6114 cell lines and a better predicted toxicity profile; consequently, we can hypothesize a better pharmacological profile of 1d respect to our lead STIRUR-41.

Although the precise role of USP-7 in cancer is not yet fully elucidated, its key involvement in regulating major cancer hallmarks and oncogenic pathways makes it an attractive and high-value target for cancer therapy.<sup>[10]</sup> The identification of novel USP-7 inhibitors endowed with an unreported chemical structure, low micromolar potency, excellent permeability, and absence of toxicity contributes to clarify the role of this enzyme in carcinogenesis and provide the basis for future studies to identify more effective USP-7 pyrazole blockers.

## 4. Experimental Section

### Chemistry

All the reagents were purchased by Alfa-Aesar and Sigma-Aldrich. DMF was reagent-grade and was dried on molecular sieves (5 Å 1/16" inch

pellets). Unless otherwise stated, all commercial reagents were used without further purification. Organic solutions were dried over anhydrous sodium sulphate. A thin layer chromatography system was utilized for routine monitoring of reaction progress and for confirming the purity of analytical samples, employing aluminum-backed silica gel plates (Merck DC-Alufolien Kieselgel 60 F254). Neat DCM or DCM/2% methanol mixture were used as the eluent, and detection of spots was achieved by UV light and/or by iodine vapors. Merck silica gel, 230–400 mesh, was used for chromatography. Flash chromatography was performed on an Isolera One instrument (Biotage, Uppsala, Sweden) using Silica gel columns. Melting points were determined on a BÜCHI M-560 (Buchi instruments, Flawil, Switzerland) apparatus and were uncorrected. Microwave apparatus: CEM Discover (CEM Corporation, Matthews, NC, USA), a single-mode microwave oven, with a max emitted power of 300 W, temperature-controlled by an optical fiber, with magnetic stirring of the sample, and an air-cooling system. <sup>1</sup>H NMR and <sup>13</sup>C NMR spectra were recorded on a JEOL JNMEXZR (400 MHz, Tokyo, Japan). Chemical shifts were reported in δ (ppm) units relative to the internal reference tetramethylsilane, and the splitting patterns were described as follows: s (singlet), bs (broad singlet), d (doublet), t (triplet), q (quartet), and m (multiplet). The first order values reported for coupling constants *J* were given in Hz. Elemental analyzes were determined by an EA1110 Analyzer, Fison Instruments (Milan, Italy). Products were considered pure when the difference between calculated and found values is ± 0.4. Compounds 3a,b were prepared as previously reported.<sup>[24]</sup>

### General Synthetic Procedure for the Preparation of Compounds 1a-b

To a dry DMF solution (5 mL) of 3a (213 mg, 1 mmol), the proper phenyl isocyanate (1.1 mmol) was added dropwise under stirring at rt. The mixture was stirred at 100 °C for 12 h, then cooled to rt, and finally, added to water (30 mL). After alkalization with NH<sub>3</sub>, the mixture was extracted with ethyl acetate (3 × 10 mL). The combined organic phases were washed with water (3 × 10 mL) and brine (3 × 10 mL), dried (MgSO<sub>4</sub>), and evaporated under reduced pressure. The crude product was purified by Flash Chromatography (Silicagel, eluent: DCM - DCM/50% Et<sub>2</sub>O-Et<sub>2</sub>O).

### Ethyl 5-Amino-1-(2-(((2-Fluorophenyl)Carbamoyl)Oxy)Propyl)-1H-Pyrazole-4-Carboxylate 1a

Yield: 33%. White solid. Mp 128–130 °C (DCM/Et<sub>2</sub>O). <sup>1</sup>H NMR (400 MHz, DMSO-*d*<sub>6</sub>) δ 1.19–1.26 (m, 6H, CHCH<sub>3</sub> + CH<sub>3</sub> ester), 4.06–4.18 (m, 4H, OCH<sub>2</sub> + NCH<sub>2</sub>), 5.06–5.12 (m, 1H, CHO), 6.23 (bs, 2H, NH<sub>2</sub>, exchangeable), 7.09–7.22 (m, 3H, arom. H), 7.46 (s, 1H, H pyraz.), 7.51–7.57 (m, 1H, arom. H), and 9.21 (bs, 1H, NH, exchangeable). <sup>13</sup>C NMR (101 MHz, DMSO-*d*<sub>6</sub>) δ 163.45, 153.19, 150.39, 138.76, 126.02, 125.90, 125.32, 124.26, 115.67, 115.47, 93.79, 69.19, 58.66, 50.56, 17.56, and 14.52. Anal calcd. for C<sub>16</sub>H<sub>19</sub>FN<sub>4</sub>O<sub>4</sub>: C: 54.85; H: 5.47; N: 15.99. Found: C: 54.57; H: 5.27; N: 15.59.

### Ethyl 5-Amino-1-(2-(((3-Fluorophenyl)Carbamoyl)Oxy)Propyl)-1H-Pyrazole-4-Carboxylate 1b

Yield: 43%. White solid. Mp 144–145 °C (DCM/Et<sub>2</sub>O). <sup>1</sup>H NMR (400 MHz, DMSO-*d*<sub>6</sub>) δ 1.18–1.26 (m, 6H, CHCH<sub>3</sub> + CH<sub>3</sub> ester), 4.07–4.18 (m, 4H, OCH<sub>2</sub> + NCH<sub>2</sub>), 5.08–5.17 (m, 1H, CHO), 6.31 (bs, 2H, NH<sub>2</sub>, exchangeable), 6.74–6.82 (m, 2H, arom. H), 7.26–7.34 (m, 2H, arom. H), 7.44 (s, 1H, H pyraz.), and 8.98 (bs, 1H, NH, exchangeable). <sup>13</sup>C NMR (101 MHz, DMSO-*d*<sub>6</sub>) δ 163.66, 152.89, 150.58, 141.15, 138.95, 130.61, 114.30, 109.11, 108.90, 105.05, 93.93, 69.03, 58.87, 50.70, 17.80, and 14.73. Anal calcd. for C<sub>16</sub>H<sub>19</sub>FN<sub>4</sub>O<sub>4</sub>: C: 54.85; H: 5.47; N: 15.99. Found: C: 54.67; H: 5.18; N: 15.89.

### Ethyl 5-Amino-1-(2-(((4-Fluorophenyl)Carbamoyl)Oxy)Propyl)-1H-Pyrazole-4-Carboxylate 1c

Yield: 53%. White solid. Mp 169–170 °C (DCM/Et<sub>2</sub>O). <sup>1</sup>H NMR (400 MHz, DMSO-*d*<sub>6</sub>) δ 1.20–1.25 (m, 6H, CHCH<sub>3</sub>+ CH<sub>3</sub> ester), 4.08–4.18 (m, 4H, OCH<sub>2</sub> + NCH<sub>2</sub>), 5.09–5.15 (m, 1H, CHO), 6.28 (bs, 2H, NH<sub>2</sub>, exchangeable), 7.01–7.12 (m, 2H, arom. H), 7.40–7.47 (m, 3H, arom. H + H pyraz.), and 9.60 (bs, 1H, NH, exchangeable). <sup>13</sup>C NMR (101 MHz, DMSO-*d*<sub>6</sub>) δ 163.96, 153.39, 150.87, 139.25, 135.95, 120.45, 115.89, 115.67, 94.24, 69.14, 59.18, 51.04, 18.16, and 15.04. Anal calcd for C<sub>16</sub>H<sub>19</sub>FN<sub>4</sub>O<sub>4</sub>: C: 54.85; H: 5.47; N: 15.99. Found: C: 54.50; H: 5.50; N: 16.26.

### Ethyl 5-Amino-1-(2-(((3-(Trifluoromethyl)Phenyl)Carbamoyl)Oxy)Propyl)-1H-Pyrazole-4-Carboxylate 1d

Yield: 43%. White solid. Mp 162–163 °C (DCM/Et<sub>2</sub>O). <sup>1</sup>H NMR (400 MHz, DMSO-*d*<sub>6</sub>) δ 1.20–1.26 (m, 6H, CHCH<sub>3</sub>+ CH<sub>3</sub> ester), 4.10–4.17 (m, 4H, OCH<sub>2</sub> + NCH<sub>2</sub>), 5.11–5.18 (m, 1H, CHO), 6.30 (bs, 2H, NH<sub>2</sub>, exchangeable), 7.29–7.33 (m, 1H, arom. H), 7.44 (s, 1H, H pyraz.), 7.46–7.52 (m, 1H, arom. H), 7.62–7.66 (m, 1H, arom. H), 7.85–7.88 (m, 1H, arom. H) and 9.94 (bs, 1H, NH, exchangeable). <sup>13</sup>C NMR (101 MHz, DMSO-*d*<sub>6</sub>) δ 163.95, 153.30, 150.91, 140.51, 139.25, 130.47, 129.85, 122.39, 119.26, 114.72, 94.23, 69.48, 59.16, 51.00, 18.07, and 15.02. Anal calcd. for C<sub>17</sub>H<sub>19</sub>F<sub>3</sub>N<sub>4</sub>O<sub>4</sub>: C: 51.00; H: 4.78; N: 13.99. Found: C: 50.76; H: 4.74; N: 13.69.

### General Synthetic Procedure for the Preparation Of Compounds 2a-d

To a dry Toluene solution (5 mL) of **3b** (227 mg, 1 mmol), the proper phenyl isocyanate (1.5 mmol) was added dropwise under stirring at rt. The mixture was stirred under microwave irradiation (max potency 300 W) at 90 °C for 7 min. Then, another equivalent of phenyl isocyanate (1.5 mmol) was added, and the solution was heated again under microwave irradiation at 90 °C for 7 min. After cooling to rt, the solvent was evaporated under reduced pressure, and the crude product was purified by Flash Chromatography (Silicagel, eluent: DCM - DCM/50% Et<sub>2</sub>O-Et<sub>2</sub>O).

### Ethyl 5-Amino-1-(2-(((2-Fluorophenyl)Carbamoyl)Oxy)Butyl)-1H-Pyrazole-4-Carboxylate 2a

Yield: 16%. White solid. Mp 97–98 °C (DCM/Et<sub>2</sub>O). <sup>1</sup>H NMR (400 MHz, DMSO-*d*<sub>6</sub>) δ 0.87 (t, *J* = 7.4 Hz, 3 H, CH<sub>3</sub>), 1.19 (t, *J* = 7.1 Hz, 3H, CH<sub>3</sub> ester), 1.48–1.72 (m, 2 H, CHCH<sub>2</sub>), 4.04–4.14 (m, 4H, OCH<sub>2</sub> + NCH<sub>2</sub>), 4.91–4.97 (m, 1H, CHO), 6.17 (bs, 2H, NH<sub>2</sub>, exchangeable), 7.05–7.18 (m, 3H, arom. H), 7.41 (s, 1H, H pyraz.), 7.48–7.54 (m, 1H, arom. H), and 9.18 (bs, 1H, NH, exchangeable). <sup>13</sup>C NMR (101 MHz, DMSO-*d*<sub>6</sub>) δ 163.97, 154.00, 150.93, 139.25, 126.63, 126.52, 125.71, 124.81, 124.78, 116.18, 94.34, 73.93, 59.18, 49.72, 24.93, 15.04, and 9.73. Anal calcd. for C<sub>17</sub>H<sub>21</sub>FN<sub>4</sub>O<sub>4</sub>: C: 56.04; H: 5.81; N: 15.38. Found: C: 55.70; H: 5.70; N: 15.45.

### Ethyl 5-Amino-1-(2-(((3-Fluorophenyl)Carbamoyl)Oxy)Butyl)-1H-Pyrazole-4-Carboxylate 2b

Yield: 27%. White solid. Mp 132–133 °C (DCM/Et<sub>2</sub>O). <sup>1</sup>H NMR (400 MHz, DMSO-*d*<sub>6</sub>) δ 0.92 (t, *J* = 7.3 Hz, 3 H, CH<sub>3</sub>), 1.22 (t, *J* = 7.1 Hz, 3 H, CH<sub>3</sub> ester), 1.48–1.72 (m, 2H, CHCH<sub>2</sub>), 4.04–4.18 (m, 4H, OCH<sub>2</sub> + NCH<sub>2</sub>), 4.97–5.08 (m, 1H, CHO), 6.28 (bs, 2H, NH<sub>2</sub>, exchangeable), 6.71–6.82 (m, 1H, arom. H), 7.15–7.36 (m, 3H, arom. H), 7.44 (s, 1H, H pyraz.), and 9.83 (bs, 1H, NH, exchangeable). <sup>13</sup>C NMR (101 MHz, DMSO-*d*<sub>6</sub>) δ 163.47, 161.14, 152.96, 150.44, 141.13, 138.71, 130.24, 114.07, 108.62, 104.84, 93.81, 73.12, 58.64, 49.18, 24.42, 14.47, and

9.24. Anal calcd. for C<sub>17</sub>H<sub>21</sub>FN<sub>4</sub>O<sub>4</sub>: C: 56.04; H: 5.81; N: 15.38. Found: C: 56.24; H: 5.76; N: 15.55.

### Ethyl 5-Amino-1-(2-(((4-Fluorophenyl)Carbamoyl)Oxy)Butyl)-1H-Pyrazole-4-Carboxylate 2c

Yield: 21%. White solid. Mp 126–127 °C (DCM/Et<sub>2</sub>O). <sup>1</sup>H NMR (400 MHz, DMSO-*d*<sub>6</sub>) δ 0.91 (t, *J* = 7.3 Hz, 3H, CH<sub>3</sub>), 1.23 (t, *J* = 7.1 Hz, 3H, CH<sub>3</sub> ester), 1.48–1.68 (m, 2H, CHCH<sub>2</sub>), 4.09–4.17 (m, 4H, OCH<sub>2</sub> + NCH<sub>2</sub>), 4.96–5.03 (m, 1H, CHO), 6.27 (bs, 2H, NH<sub>2</sub>, exchangeable), 7.06–7.12 (m, 2H, arom. H), 7.39–7.45 (m, 3H, arom. H + H pyraz.), and 9.63 (bs, 1H, NH, exchangeable). <sup>13</sup>C NMR (101 MHz, DMSO-*d*<sub>6</sub>) δ 163.44, 153.14, 150.39, 138.68, 135.47, 119.89, 115.36, 115.14, 93.75, 72.87, 58.65, 49.17, 24.43, 14.51, and 9.26. Anal calcd. for C<sub>17</sub>H<sub>21</sub>FN<sub>4</sub>O<sub>4</sub>: C: 56.04; H: 5.81; N: 15.38. Found: C: 56.30; H: 5.59; N: 15.14.

### Ethyl 5-Amino-1-(2-(((3-(Trifluoromethyl)Phenyl)Carbamoyl)Oxy)Butyl)-1H-Pyrazole-4-Carboxylate 2d

Yield: 24%. White solid. Mp 148–149 °C (DCM/Et<sub>2</sub>O). <sup>1</sup>H NMR (400 MHz, DMSO-*d*<sub>6</sub>) δ 0.92 (t, *J* = 7.4 Hz, 3H, CH<sub>3</sub>), 1.22 (t, *J* = 7.1 Hz, 3H, CH<sub>3</sub> ester), 1.50–1.71 (m, 2H, CHCH<sub>2</sub>), 4.10–4.17 (m, 4H, OCH<sub>2</sub> + NCH<sub>2</sub>), 5.00–5.07 (m, 1H, CHO), 6.28 (bs, 2H, NH<sub>2</sub>, exchangeable), 7.29–7.33 (m, 1H, arom. H), 7.43 (s, 1H, H pyraz.), 7.46–7.51 (m, 1H, arom. H), 7.62–7.66 (m, 1H, arom. H), 7.85–7.89 (m, 1H, arom. H), and 9.96 (bs, 1H, NH, exchangeable). <sup>13</sup>C NMR (101 MHz, DMSO-*d*<sub>6</sub>) δ 163.23, 152.85, 150.23, 139.84, 138.48, 129.71, 129.14, 129.14, 121.64, 118.47, 113.98, 93.55, 73.04, 58.41, 48.95, 30.49, 24.17, 14.26, and 9.06. Anal calcd. for C<sub>18</sub>H<sub>21</sub>F<sub>3</sub>N<sub>4</sub>O<sub>4</sub>: C: 52.17; H: 5.11; N: 13.52. Found: C: 52.04; H: 4.98; N: 13.85.

### X-ray Crystallography

Diffraction-quality crystals of **1b** were grown as colorless plates through slow evaporation of a chloroform/methanol solution of the compound. X-ray intensity data were collected at 293(2) K using a Rigaku XtaLAB Synergy diffractometer (Rigaku, Tokyo, Japan), equipped with a microfocus PhotonJet Mo-Kα source and a hybrid pixel array detector. The data were obtained through omega scans with a step size of 0.5° and an exposure time of 40 s per frame. A total of 21 414 Bragg reflections were recorded, revealing a metrically orthorhombic unit cell. Systematic absence analysis suggested the space group Pca2<sup>1</sup>. Intensity data were integrated and empirically corrected for Lorentz-polarization and absorption effects using CrysAlisPro 1.171.42.58a (Rigaku Oxford Diffraction/Agilent Technologies UK Ltd.). The structure was solved by direct methods with SIR2019/3<sup>[33]</sup> and refined through iterative full-matrix least-squares refinement on Fo2 and ΔF synthesis using SHELXL-2019/3<sup>[34]</sup> within the WinGX suite (WinGX v.2023.1).<sup>[35]</sup> Hydrogen atoms were placed in calculated positions according to their expected geometries and were refined using a riding model with fixed isotropic thermal parameters (1.2 and 1.5 Ueq of the parent atom for aromatic/methylene/methine and methyl groups, respectively). Structural analysis was performed using PARST<sup>[36]</sup> and Mercury 2024.3.0;<sup>[37]</sup> graphical representations were generated with Mercury. HS generation was carried out with CrystalExplorer21.<sup>[38]</sup> Crystal data and structure refinement details are shown in Table S2, Supporting Information.

Deposition Number 2421400 (for compound **1b**) <https://www.ccdc.cam.ac.uk/services/structures?id=doi:10.1002/cmdc.202500185> contains the supplementary crystallographic data for this paper. These data are provided free of charge by the joint Cambridge Crystallographic Data Centre and Fachinformationszentrum Karlsruhe <http://www.ccdc.cam.ac.uk/structures> Access Structures service.

## Ub-AMC Assay

In vitro enzymatic inhibition was measured using the USP-7 inhibitor screening assay kit (catalog #79,256, BPS Bioscience, San Diego, CA, USA) according to the manufacturer's instructions. Briefly, compound stock solutions were prepared in DMSO and diluted tenfold to obtain the working solutions. Then, these solutions and the vehicle control were added to the black 384-wells plate, together with the USP-7 enzyme, previously diluted as required by the manufacturer, and incubated at rt for 30 min. Then, the Ub-AMC substrate was diluted 400-fold and added to the plate, followed by incubation at rt for 30 min. The final DMSO amount in each well was 1%. The fluorescence signal (excitation = 350 nm, emission = 460 nm) was recorded using the Victor Nivo microplate reader (Revvity, Waltham, MA, USA).  $IC_{50}$  was calculated by subtracting Ub-AMC background from each value. The results are expressed as means  $\pm$  SEM of at least three independent experiments. For  $IC_{50}$  determination, the curves were obtained using GraphPad Prism 7 (San Diego, CA, USA).

## Antiproliferative Activity

To perform the MTT assay, SK-BR3 (breast adenocarcinoma, Biologic Bank and Cell Factory, IRCCS Policlinico San Martino, Genoa, Italy), MCF-7 (breast adenocarcinoma, Biologic Bank and Cell Factory, IRCCS Policlinico San Martino, Genoa, Italy), SK-Mel28 (skin melanoma, Biologic Bank and Cell Factory, IRCCS Policlinico San Martino, Genoa, Italy), Hep-G2 (hepatocellular carcinoma, ATCC, Manassas, VA), SKOV-3 (ovarian adenocarcinoma, ATCC, Manassas, VA), MDA-MB-231 (breast adenocarcinoma, Biologic Bank and Cell Factory, IRCCS Policlinico San Martino, Genoa, Italy), HeLa (cervical adenocarcinoma, Biologic Bank and Cell Factory, IRCCS Policlinico San Martino, Genoa, Italy), A549 (lung adenocarcinoma, ATCC, Manassas, VA), and GM-6114 (normal human embryonic fibroblast, ATCC, Manassas, VA) cell lines were cultured in Dulbecco's modified eagle medium (DMEM added with 10% Fetal bovine serum, 2 mM Glutamine, and 1% pen-strep) and incubated in a humidified environment at 37 °C with 5% CO<sub>2</sub>. Reagents were acquired from EuroClone (Milan, Italy). All chemical compounds were dissolved in DMSO to give a 10 mM stock solution. Then, after an intermediate dilution in growth medium, they were added to the cultured cells at a final working concentration of 10  $\mu$ M and incubated for 48 h. At the end of the incubation, 30  $\mu$ L of MTT (3-(4,5-dimethyl-2-thiazolyl)-2,5-diphenyl-2H-tetrazolium bromide) at a concentration of 2 mg mL<sup>-1</sup> in phosphate buffered saline (PBS) were added into each well and further incubated for 4 h. Finally, the supernatants were removed and 100  $\mu$ L well of DMSO were added to each well to dissolve the Formazan precipitates. After 20 min, plates were read at 570 nm. Results are expressed as the percentage of the control samples where cells have been treated with the same amount of DMSO but without any chemical compound. The assay was repeated three times, and a single compound was tested six times. Means and standard deviations were calculated.

## PAMPA Assays

The assay was prepared as follows: 300  $\mu$ L of PBS pH 7.4 (5% DMSO) was placed in the acceptor wells. A phosphatidylcholine (PC) solution was obtained by dissolving and vortexing PC at 1% w/v in dodecane and solubilized using an ultrasound bath until a clear solution was obtained. 5 mL of this solution was deposited on the membrane portion of the donor well. 150  $\mu$ L of each molecule, at 100–250  $\mu$ M final concentration (5% DMSO), was pipetted in the acceptor wells. The acceptor (Multiscreen transport Receiver Plate, 96-well, polystyrene, Millipore) and donor plates (Multiscreen Filter Plates, IP, 0.45 mm, clear, hydrophobic PVDF, Millipore) were subsequently assembled and incubated for 5 h under gentle orbital shaking. The experiment was conducted in duplicate. Lucifer yellow was used

as a negative control to establish the integrity of the membrane, quantifying its concentration in both acceptor and donor solutions using fluorescence. Propranolol and Furosemide were used as positive and negative controls. Acceptor, donor, and equilibrium solutions, along with the original 100–250  $\mu$ M stock solutions, were analyzed by UV detector at 250 nm for compound **1d**, 280 nm for propranolol, and 275 nm for furosemide (Victor Nivo, Revvity, USA). The results are expressed as means  $\pm$  SEM of at least three independent experiments.

## Computational Studies

The calculations were run on a Linux PC (Intel processor Core i7-2600 CPU@3.40 GHz).

## Docking Studies

The molecular structures of compounds (**R**)-**1d** and (**S**)-**1d** were built by MOE2009.10 (builder module), parameterized by MMFF94x force field, and their docking poses within USP-7 were calculated by Autodock 4.2.<sup>[31]</sup> After the removal of water molecules and ligand atoms from the crystal structure of USP-7N terminal domain (PDB ID: 5N9T),<sup>[32]</sup> polar hydrogen and Gasteiger–Huckel charges were added. The ligand root was defined automatically. A 60  $\times$  60  $\times$  60  $\text{Å}$  grid (grid spacing 0.375  $\text{Å}$ ) was centered in the binding site of the cocrystallized ligand, and electrostatic and affinity maps for each atom type of the ligand were calculated. The docking search was performed over 100 conformers using the Genetic Algorithm Local Search protocol as implemented in Autodock (population size: 50; rate of gene mutation: 0.02; rate of crossover: 0.8). The docking poses were clustered (rmsd: 2.0  $\text{Å}$ ) and the best conformation of the low-energy highest populated cluster was selected as the binding conformation. Model analysis was carried out using the CCP4 program suite.<sup>[39]</sup>

## Molecular Dynamics Studies

The coordinates of (**S**)-**1d** docking pose were parameterized by CHARMM-GUI.<sup>[40]</sup> The molecular structure of the USP-7 enzyme was processed and parameterized by the VMD package version 1.9.3 (Automatic PSF building module).<sup>[41]</sup> The protein–ligand complex was assembled, and a solvation box including the whole complex (max box padding:  $X = 7$ ;  $y = 0$ ,  $z = 7$ ) was defined. The molecular dynamics simulation was carried out by the software NAMD 2.14, developed by the Theoretical and Computational Biophysics Group in the Beckman Institute for Advanced Science and Technology at the University of Illinois at Urbana-Champaign.<sup>[42]</sup> The following parameters were adopted: run = 5,010,000; time step = 2; temperature = 310; restartfreq = 50. VMD “RMSD trajectory tool” and “Hydrogen bonds” were used to analyze the trajectory file.

## Acknowledgements

This research was funded by Università degli Studi di Genova, grant Fondi di Ricerca di Ateneo (FRA). C.R., E.I., and M.P. acknowledge the support of the Italian Minister of Health (Ricerca Corrente). The authors thank Dr. M. Anzaldi, F. Rapetti, and R. Raggio for spectral recording and elemental analysis and M. Massone for helpful discussion.

Open access publishing facilitated by Università degli Studi di Genova, as part of the Wiley - CRUI-CARE agreement.

## Conflict of Interest

The authors declare no conflict of interest.

## Author Contributions

**Matteo Lusardi:** investigation (lead); writing—review and editing (Equal). **Elva Morretta:** data curation (equal); investigation (equal); methodology (equal). **Andrea Spallarossa:** investigation (equal); methodology (equal); writing—review and editing (equal). **Maria Chiara Monti:** methodology (equal); supervision (equal); writing—review and editing (equal). **Camillo Rosano:** supervision (supporting); **Erika Iervasi:** data curation (equal); methodology (equal). **Marco Ponassi:** investigation (equal); methodology (equal); supervision (equal). **Matteo Mori:** investigation (equal); methodology (equal); writing—review and editing (equal). **Fiorella Meneghetti:** methodology (equal); supervision (equal); writing—review and editing (equal). **Chiara Brullo:** conceptualization (lead); data curation (lead); investigation (lead); writing—original draft (lead).

## Data Availability Statement

The data that support the findings of this study are available from the corresponding author upon reasonable request.

**Keywords:** antiproliferative agents · computational simulations · pyrazole compounds · single crystal X-ray diffraction · ubiquitin-specific protease 7 inhibitors

- [1] A. Georges, E. Marcon, J. Greenblatt, L. Frappier, *Sci. Rep.* **2019**, *9*, 15664.
- [2] Z. Wang, W. Kang, Y. You, J. Pang, H. Ren, Z. Suo, H. Liu, Y. Zheng, *Front. Pharmacol.* **2019**, *10*, 427.
- [3] H.-B. Park, S. Hwang, K.-H. Baek, *Cell Death Dis.* **2022**, *13*, 698.
- [4] G. Saha, S. Roy, M. Basu, M. K. Ghosh, *Biochim. Biophys. Acta Rev. Cancer.* **2023**, *1878*, 188903.
- [5] S.-M. Qi, G. Cheng, X.-D. Cheng, Z. Xu, B. Xu, W.-D. Zhang, J.-J. Qin, *Front. Cell Dev. Biol.* **2020**, *8*, 233.
- [6] T. An, Y. Gong, X. Li, L. Kong, P. Ma, L. Gong, H. Zhu, C. Yu, J. Liu, H. Zhou, B. Mao, Y. Li, *Biochem. Pharmacol.* **2017**, *131*, 29.
- [7] A. Collieran, P. E. Collins, C. O'Carroll, A. Ahmed, X. Mao, B. McManus, P. A. Kiely, E. Burstein, R. J. Carmody, *Proc. Natl. Acad. Sci. U.S.A.* **2013**, *110*, 618.
- [8] J. van Loosdregt, V. Fleskens, J. Fu, A. B. Brenkman, C. P. J. Bekker, C. E. G. M. Pals, J. Meerding, C. R. Berkers, J. Barbi, A. Gröne, A. J. A. M. Sijts, M. M. Maurice, E. Kalkhoven, B. J. Prakken, H. Ovaa, F. Pan, D. M. W. Zaiss, P. J. Coffey, *Immunity* **2013**, *39*, 259.
- [9] M. S. Song, L. Salmena, A. Carracedo, A. Egia, F. Lo-Coco, J. Teruya-Feldstein, P. P. Pandolfi, *Nature* **2008**, *455*, 813.
- [10] G. J. Valles, I. Bezsonova, R. Woodgate, N. W. Ashton, *Front. Cell Dev. Biol.* **2020**, *8*, 717.
- [11] J. Lu, H. Zhao, C. Yu, Y. Kang, X. Yang, *Front. Pharmacol.* **2021**, *12*, 648491.
- [12] M. Ye, J. He, J. Zhang, B. Liu, X. Liu, L. Xie, M. Wei, R. Dong, K. Li, D. Ma, K. Dong, *Cancer Biomark.* **2021**, *31*, 107.
- [13] S. Collaud, V. Tischler, A. Atanassoff, T. Wiedl, P. Komminoth, C. Oehlschlegel, W. Weder, A. Soltermann, *BMC Cancer* **2015**, *15*, 74.
- [14] D. Masuya, C. Huang, D. Liu, T. Nakashima, H. Yokomise, M. Ueno, N. Nakashima, S. Sumitomo, *J. Pathol.* **2006**, *208*, 724.
- [15] P. Liu, Z. Chen, Y. Guo, Q. He, C. Pan, *Eur. J. Med. Chem.* **2025**, *287*, 117324.
- [16] P. Li, Y. Liu, H.-M. Liu, *Expert Opin. Ther. Pat.* **2022**, *32*, 753.
- [17] R. I. Oliveira, R. A. Guedes, J. A. R. Salvador, *Front. Chem.* **2022**, *10*, 1005727.
- [18] L. Nininahazwe, B. Liu, C. He, H. Zhang, Z.-S. Chen, *Drug Discov. Today* **2021**, *26*, 490.
- [19] B. M. Kessler, *Expert Opin. Ther. Pat.* **2014**, *24*, 597.
- [20] A. P. Turnbull, S. Ioannidis, W. W. Krajewski, A. Pinto-Fernandez, C. Heride, A. C. L. Martin, L. M. Tonkin, E. C. Townsend, S. M. Buker, D. R. Lancia, J. A. Caravella, A. V. Toms, T. M. Charlton, J. Lahdenranta, E. Wilker, B. C. Follows, N. J. Evans, L. Stead, C. Alli, V. V. Zarayskiy, A. C. Talbot, A. J. Buckmelter, M. Wang, C. L. McKinnon, F. Saab, J. F. McGouran, H. Century, M. Gersch, M. S. Pittman, C. G. Marshall, T. M. Raynham, M. Simcox, L. M. D. Stewart, S. B. McLoughlin, J. A. Escobedo, K. W. Bair, C. J. Dinsmore, T. R. Hammonds, S. Kim, S. Urbé, M. J. Clague, B. M. Kessler, D. Komander, *Nature* **2017**, *550*, 481.
- [21] O. Tavana, W. Gu, *J. Mol. Cell. Biol.* **2017**, *9*, 45.
- [22] I. Lamberto, X. Liu, H.-S. Seo, N. J. Schauer, R. E. Iacob, W. Hu, D. Das, T. Mikhailova, E. L. Weisberg, J. R. Engen, K. C. Anderson, D. Chauhan, S. Dhe-Paganon, S. J. Buhrlage, *Cell. Chem. Biol.* **2017**, *24*, 1490.
- [23] I. E. Wertz, J. M. Murray, *Drug Discov. Today Technol.* **2019**, *31*, 109.
- [24] O. Bruno, C. Brullo, F. Bondavalli, S. Schenone, S. Spisani, M. S. Falzarano, K. Varani, E. Barocelli, V. Ballabeni, C. Giorgio, M. Tognolini, *Bioorg. Med. Chem.* **2009**, *17*, 3379.
- [25] B. Marengo, E. Meta, C. Brullo, C. D. Ciucis, R. Colla, A. Speciale, O. Garbarino, O. Bruno, C. Domenicotti, *Oncotarget* **2023**, *14*, 129.
- [26] E. Morretta, C. Brullo, R. Belvedere, A. Petrella, A. Spallarossa, M. C. Monti, *Int. J. Mol. Sci.* **2023**, *24*, 9200.
- [27] E. Meta, C. Brullo, A. Sidibe, B. A. Imhof, O. Bruno, *Eur. J. Med. Chem.* **2017**, *133*, 24.
- [28] M. Lusardi, B. Wehrle-Haller, A. Sidibe, M. Ponassi, E. Iervasi, C. Rosano, C. Brullo, A. Spallarossa, *Eur. J. Med. Chem.* **2023**, *260*, 115727.
- [29] A. Daina, O. Michielin, V. Zoete, *Sci. Rep.* **2017**, *7*, 42717.
- [30] M. N. Drwal, P. Banerjee, M. Dunkel, M. R. Wettig, R. Preissner, *Nucleic Acids Res.* **2014**, *42*, W53.
- [31] G. M. Morris, R. Huey, W. Lindstrom, M. F. Sanner, R. K. Belew, D. S. Goodsell, A. J. Olson, *J. Comput. Chem.* **2009**, *30*, 2785.
- [32] G. Gavory, C. R. O'Dowd, M. D. Helm, J. Flasz, E. Arkoudis, A. Dossang, C. Hughes, E. Cassidy, K. McClelland, E. Odrzywol, N. Page, O. Barker, H. Miel, T. Harrison, *Nat. Chem. Biol.* **2018**, *14*, 118.
- [33] M. C. Burla, R. Caliendo, B. Carrozzini, G. L. Cascarano, C. Cuocci, C. Giacobozzo, M. Mallamo, A. Mazzone, G. Polidori, *J. Appl. Crystallogr.* **2015**, *48*, 306.
- [34] G. M. Sheldrick, *Acta Crystallogr. C Struct. Chem.* **2015**, *71*, 3.
- [35] L. J. Farrugia, *J. Appl. Crystallogr.* **2012**, *45*, 849.
- [36] M. Nardelli, *Comput. Chem.* **1983**, *7*, 95.
- [37] C. F. Macrae, I. Sovago, S. J. Cottrell, P. T. A. Galek, P. McCabe, E. Pidcock, M. Platings, G. P. Shields, J. S. Stevens, M. Towler, P. A. Wood, *J. Appl. Crystallogr.* **2020**, *53*, 226.
- [38] P. R. Spackman, M. J. Turner, J. J. McKinnon, S. K. Wolff, D. J. Grimwood, D. Jayatilaka, M. A. Spackman, *J. Appl. Crystallogr.* **2021**, *54*, 1006.
- [39] M. D. Winn, C. C. Ballard, K. D. Cowtan, E. J. Dodson, P. Emsley, P. R. Evans, R. M. Keegan, E. B. Krissinel, A. G. W. Leslie, A. McCoy, S. J. McNicholas, G. N. Murshudov, N. S. Pannu, E. A. Potterton, H. R. Powell, R. J. Read, A. Vagin, K. S. Wilson, *Acta Crystallogr. D Biol. Crystallogr.* **2011**, *67*, 235.
- [40] S. Jo, T. Kim, V. G. Iyer, W. Im, *J. Comput. Chem.* **2008**, *29*, 1859.
- [41] W. Humphrey, A. Dalke, K. Schulten, *J. Molec. Graphics* **1996**, *14*, 33.
- [42] J. C. Phillips, D. J. Hardy, J. D. C. Maia, J. E. Stone, J. V. Ribeiro, R. C. Bernardi, R. Buch, G. Fiorin, J. Hénin, W. Jiang, R. McGreevy, M. C. R. Melo, B. K. Radak, R. D. Skeel, A. Singharoy, Y. Wang, B. Roux, A. Aksimentiev, Z. Luthey-Schulten, L. V. Kalé, K. Schulten, C. Chipot, E. Tajkhorshid, *J. Chem. Phys.* **2020**, *153*, 044130.

Manuscript received: March 6, 2025

Revised manuscript received: May 26, 2025

Version of record online: June 24, 2025

# ChemMedChem

## Supporting Information

### Targeting USP-7 With Novel 5-Amino-Pyrazole Inhibitors: Design, Synthesis and Biological Evaluation

Matteo Lusardi,<sup>[a,b]</sup> Elva Morretta,<sup>[c]</sup> Andrea Spallarossa,<sup>[a]</sup> Maria Chiara Monti,<sup>[c]</sup> Camillo Rosano,<sup>[d]</sup> Erika Iervasi,<sup>[d]</sup> Marco Ponassi,<sup>[d]</sup> Matteo Mori,<sup>[e]</sup> Fiorella Meneghetti,<sup>[e]</sup> Chiara Brullo\*<sup>[a]</sup>

<sup>[a]</sup>Department of Pharmacy, University of Genova, Viale Benedetto XV, 3, 16132 Genova, Italy

<sup>[b]</sup>Molecular Modeling and Drug Discovery Laboratory, Istituto Italiano di Tecnologia, Via Morego, 30, 16163, Genova, Italy.

<sup>[c]</sup>Department of Pharmacy, University of Naples "Federico II", Via Domenico Montesano, 49, 80131 Napoli, Italy.

<sup>[d]</sup>IRCCS Ospedale Policlinico San Martino, L.go. R. Benzi, 10 I-16132 Genova, Italy.

<sup>[e]</sup>Department of Pharmaceutical chemistry, University of Milan, Via Mangiagalli, 25, 20133 Milano, Italy.

\* Corresponding author: chiara.brullo@unige.it

## Table of contents

**Table S1.** Analysis of the intermolecular contacts on HS-1 of **1b**.

**Table S2.** Crystal data and structure refinement details for **1b**.

**Table S3.** Predicted pharmacokinetics and drug-like properties of compounds **1d** and **STIRUR-41**.

**Table S4.** Interatomic distances (cutoff distance = 4.00 Å) in the USP-7/1d(R) complex.

**Table S5.** Interatomic distances (cutoff distance = 4.00 Å) in the USP-7/1d(S) complex-

**Figure S1.** Dose response curve of compounds **1a-d** on USP-7 enzyme

**Figure S2.** <sup>1</sup>H (400 MHz, DMSO-d<sub>6</sub>) spectrum of compound **1a**.

**Figure S3.** <sup>13</sup>C (101 MHz, DMSO-d<sub>6</sub>) spectrum of compound **1a**.

**Figure S4.** <sup>1</sup>H (400 MHz, DMSO-d<sub>6</sub>) spectrum of compound **1b**.

**Figure S5.** <sup>13</sup>C (101 MHz, DMSO-d<sub>6</sub>) spectrum of compound **1b**.

**Figure S6.** <sup>1</sup>H (400 MHz, DMSO-d<sub>6</sub>) spectrum of compound **1c**.

**Figure S7.** <sup>13</sup>C (101 MHz, DMSO-d<sub>6</sub>) spectrum of compound **1c**.

**Figure S8.** <sup>1</sup>H (400 MHz, DMSO-d<sub>6</sub>) spectrum of compound **1d**.

**Figure S9.** <sup>13</sup>C (101 MHz, DMSO-d<sub>6</sub>) spectrum of compound **1d**.

**Figure S10.** <sup>1</sup>H (400 MHz, DMSO-d<sub>6</sub>) spectrum of compound **2a**.

**Figure S11.** <sup>13</sup>C (101 MHz, DMSO-d<sub>6</sub>) spectrum of compound **2a**.

**Figure S12.** <sup>1</sup>H (400 MHz, DMSO-d<sub>6</sub>) spectrum of compound **2b**.

**Figure S13.** <sup>13</sup>C (101 MHz, DMSO-d<sub>6</sub>) spectrum of compound **2b**.

**Figure S14.** <sup>1</sup>H (400 MHz, DMSO-d<sub>6</sub>) spectrum of compound **2c**.

**Figure S15.** <sup>13</sup>C (101 MHz, DMSO-d<sub>6</sub>) spectrum of compound **2c**.

**Figure S16.** <sup>1</sup>H (400 MHz, DMSO-d<sub>6</sub>) spectrum of compound **2d**.

**Figure S17.** <sup>13</sup>C (101 MHz, DMSO-d<sub>6</sub>) spectrum of compound **2d**.

**Table S1.** Analysis of the intermolecular contacts on HS-1 of **1b**. Contact values were computed with *CrystalExplorer*. Surface contributions and enrichment ratios were calculated according to Jelsch.

Atoms	H	C	N	O	F
Surface (%)	70.3	11.1	4.8	8.6	5.5
Contacts (%)					
H	47.0				
C	13.4	3.4			
N	8.0	0.5	0.4		
O	15.7	1.2	0.2	0	
F	9.5	0.2	0	0	0.6
Enrichments					
H	0.95				
C	0.86	<b>2.76</b>			
N	<b>1.19</b>	0.50	-		
O	<b>1.30</b>	0.63	-	-	
F	<b>1.23</b>	0.16	-	-	-

**Table S2.** Crystal data and structure refinement details for **1b**.

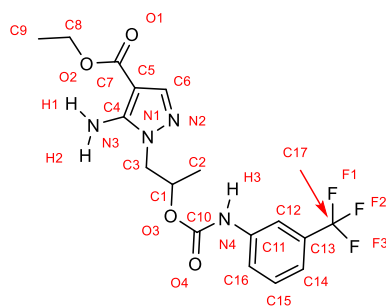
Identification code	<b>1b</b>
Empirical formula (sum)	C <sub>32</sub> H <sub>38</sub> F <sub>2</sub> N <sub>8</sub> O <sub>8</sub>
Formula weight (sum)	700.70
Temperature (K)	293(2)
Wavelength (Å)	0.71073
Crystal system	Orthorhombic
Space group	Pca2 <sub>1</sub>
Unit cell dimensions (Å/°)	<i>a</i> = 13.5011(6) <i>b</i> = 30.4561(14) <i>c</i> = 8.6895(4)
Volume (Å <sup>3</sup> )	3573.0(3)
Z	4
Density calcd. (Mg/m <sup>3</sup> )	1.303
Abs. coefficient (mm <sup>-1</sup> )	0.102
F(000)	1472
Crystal size (mm <sup>3</sup> )	0.7 x 0.2 x 0.02
θ range data collection (°)	1.650 to 26.372
Index ranges	-13 ≤ <i>h</i> ≤ 16, -38 ≤ <i>k</i> ≤ 37, -6 ≤ <i>l</i> ≤ 10
Reflections collected	21414
Independent reflections	6268 [R <sub>int</sub> = 0.0411]
Completeness to θ <sub>max</sub> (%)	99.9
Refinement method	Full-matrix least-squares on F <sup>2</sup>
Data/restraints/parameters	6268/1/451
Goodness-of-fit on F <sup>2</sup>	1.021
Final R indices [I > 2σ(I)]	R1 = 0.0462, wR2 = 0.1114
R indices (all data)	R1 = 0.0800, wR2 = 0.1306
Flack parameter	-0.2(7)
Largest diff. peak/hole (e·Å <sup>-3</sup> )	0.167 and -0.159
CCDC deposition number	2421400

**Table S3.** Predicted pharmacokinetics and drug-like properties of compounds **1d** and **STIRUR-41**

	<b>STIRUR-41</b>	<b>1d</b>
<b>Physicochemical Prop.</b>		
MW (g/mol)	350.34	400.35
Fraction Csp <sup>3</sup>	0.31	0.35
Rotatable bonds	9	10
H-bond acceptors	6	8
H-bond donors	3	2
TPSA <sup>a</sup> (Å <sup>2</sup> )	105.48	108.47
<b>Lipophilicity</b>		
LogP <sup>b</sup>	1.68	3.18
<b>Water solubility</b>		
Solubility (mg/mL) <sup>c</sup>	5.53 x 10 <sup>-1</sup>	4.43 x 10 <sup>-2</sup>
Solubility class	soluble	soluble
<b>Pharmacokinetics</b>		
GI absorption	hight	hight
BBB permeant	no	no
Pgp substrate	yes	no
CYP1A2 inhibitor	no	yes
CYP2C19 inhibitor	no	yes
CYP2C9 inhibitor	no	yes
CYP2D6 inhibitor	no	no
CYP3A4 inhibitor	no	no
<b>Druglikeness</b>		
Lipinski violations	0	0
<b>Medicinal chemistry</b>		
PAINS alerts	0	0
Brenk alerts	0	1

<sup>a</sup> Topological Polar Surface Area. <sup>b</sup> Predicted according to XLOGP3 program. <sup>c</sup> Values predicted by ESOL method.

**Table S4.** Interatomic distances (cutoff distance = 4.00 Å) in the USP-7/1d(R) complex. \*\*\* = H bond

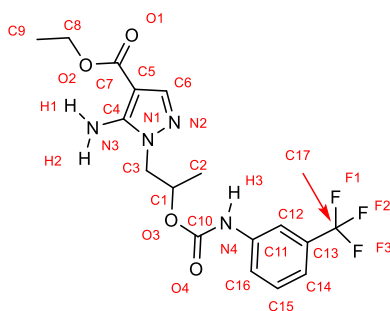


LIGAND ATOM	RESIDUE/ATOM	DISTANCE (Å)
C1	295(ASP)/OD1	3.29
	295(ASP)/CG	3.92
	297(GLN)/OE1	3.92
C2	405(GLN)/CB	3.25
	405(GLN)/CG	3.73
	406(LEU)/O	3.80
	297(GLN)/OE1	3.40
C3	297(GLN)/NE2	3.93
	296(VAL)/CG1	3.52
N1	295(ASP)/OD1	3.90
	296(VAL)/CG1	3.71
	296(VAL)/N	3.51
C4	295(ASP)/OD1	3.46
	295(ASP)/OD1	2.94
	295(ASP)/OD1	3.73
C5	224(TYR)/CD2	3.26
	224(TYR)/CE2	3.36
	296(VAL)/N	3.35
	296(VAL)/CB	3.90
N2	296(VAL)/CG1	3.19
	295(ASP)/C	3.99
	296(VAL)/N	2.96
	296(VAL)/CA	3.57
	296(VAL)/CB	3.11
N3	409(PHE)/CB	3.64
	295(ASP)/OD1	2.68
	409(PHE)/CD2	3.68
H1	295(ASP)/CG	3.90
	409(PHE)/CB	3.75
	295(ASP)/OD1	1.95
	409(PHE)/CD2	3.89
	295(ASP)/CG	3.13
H2	295(ASP)/OD2	3.90
	409(PHE)/CB	3.03
	409(PHE)/CG	3.63
	295(ASP)/OD1	3.57

	409(PHE)/CD2	3.62
C7	294(HIS)/O	3.93
	461(HIS)/NE2	3.28
O1	461(HIS)/CE1	3.23
	461(HIS)/CD2	3.53
	461(HIS)/NE2	2.66 ***
O2	224(TYR)/CE2	3.82
	291(PHE)/O	3.60
	294(HIS)/C	3.71
	294(HIS)/O	2.74
	461(HIS)/NE2	3.14
C8	461(HIS)/CE1	3.74
	291(PHE)/O	3.80
	294(HIS)/C	3.73
	294(HIS)/O	3.05
	461(HIS)/NE2	3.24
	292(MET)/C	3.83
	292(MET)/O	3.18
C9	294(HIS)/C	3.51
	294(HIS)/O	3.28
	295(ASP)/N	3.72
	295(ASP)/CA	3.91
	292(MET)/O	3.88
	295(ASP)/OD1	3.19
	295(ASP)/CG	3.77
O3	409(PHE)/CB	3.94
	406(LEU)/O	3.77
	295(ASP)/OD1	3.77
C10	409(PHE)/N	3.57
	409(PHE)/CB	3.45
	406(LEU)/O	3.88
O4	407(MET)/C	3.35
	408(ARG)/N	2.99
	408(ARG)/CA	3.96
	408(ARG)/C	3.92
	409(PHE)/N	3.03
	409(PHE)/CA	3.85
	409(PHE)/CB	3.77
	406(LEU)/C	3.96
	406(LEU)/O	3.17
	407(MET)/CA	3.12
N4	409(PHE)/CB	3.39
	295(ASP)/OD1	3.09
	295(ASP)/CG	3.83
	295(ASP)/OD2	4.00
	409(PHE)/O	3.85
H3	409(PHE)/CB	3.64

	295(ASP)/OD1	2.15 ***
	295(ASP)/CG	3.04
	295(ASP)/OD2	3.41
C11	409(PHE)/CB	3.73
	295(ASP)/OD1	3.82
	409(PHE)/O	3.10
C12	295(ASP)/OD1	3.85
	295(ASP)/OD2	3.80
	409(PHE)/O	3.21
C13	409(PHE)/O	3.28
C14	409(PHE)/O	3.27
C15	409(PHE)/O	3.17
C16	409(PHE)/C	4.00
	409(PHE)/O	3.08
C17	418(ASN)/ND2	3.43
	418(ASN)/CG	3.84
	418(ASN)/OD1	3.74
F1	418(ASN)/ND2	3.01
	418(ASN)/CG	3.14
	418(ASN)/OD1	2.70
F3	418(ASN)/ND2	2.65
	418(ASN)/CG	3.45
	418(ASN)/OD1	3.78

**Table S5.** Interatomic distances (cutoff distance = 4.00 Å) in the USP-7/1d(S) complex. \*\*\* = H bond

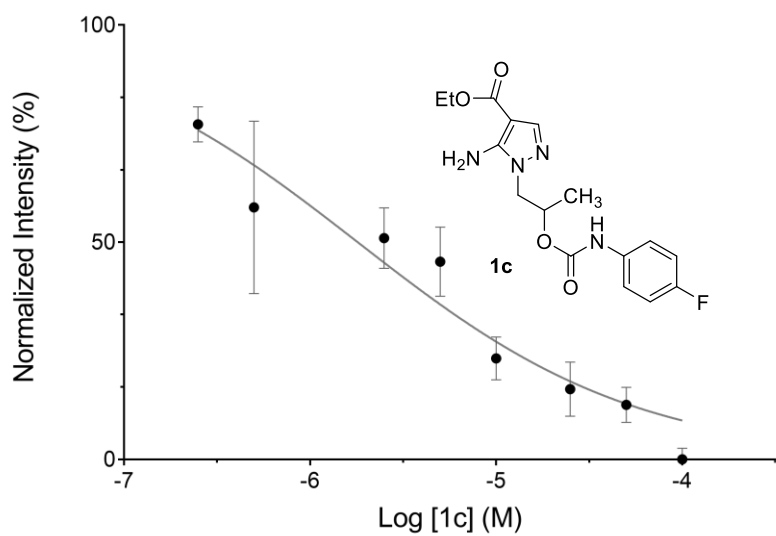
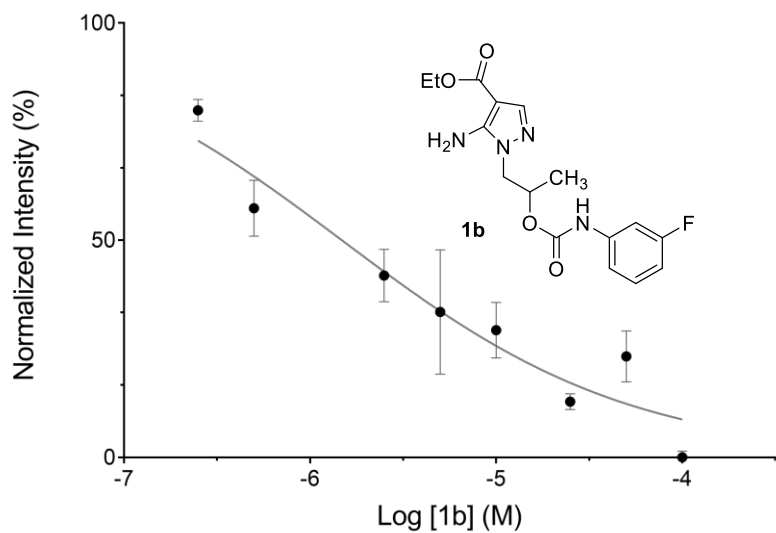
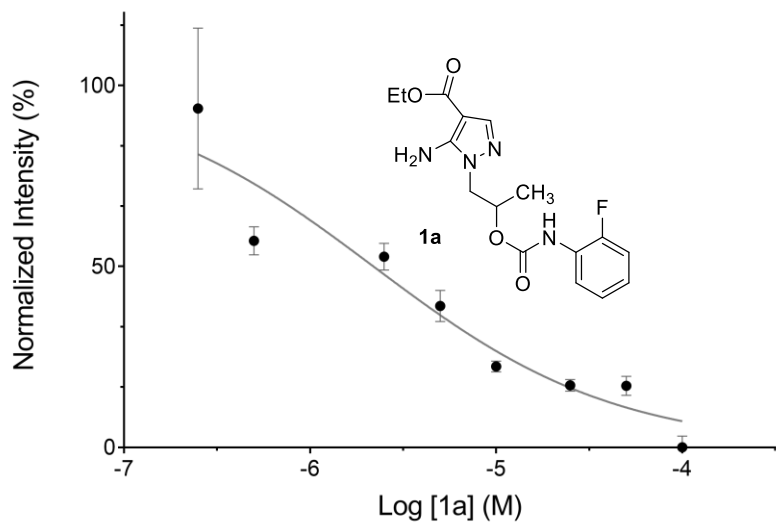


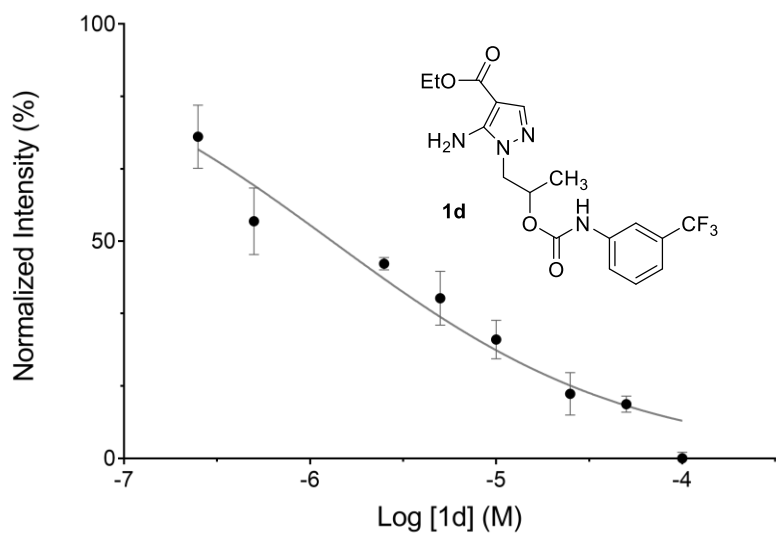
LIGAND ATOM	RESIDUE/ATOM	DISTANCE (Å)
C1	295(ASP)/OD1	3.88
C2	405(GLN)/CB	3.48
	405(GLN)/CG	3.96
	406(LEU)/O	3.71
	297(GLN)/OE1	3.60
C3	296(VAL)/CG1	3.51
	295(ASP)/CA	3.84
	296(VAL)/N	3.43
	295(ASP)/OD1	3.00
	295(ASP)/CB	3.46
	295(ASP)/CG	3.57
	297(GLN)/OE1	3.46
N1	296(VAL)/CG1	3.91
	295(ASP)/CA	3.84
	296(VAL)/N	3.38
	295(ASP)/OD1	3.25
	295(ASP)/CB	3.99
C4	295(ASP)/OD1	3.14
C6	224(TYR)/CD2	3.38
	224(TYR)/CE2	3.72
N2	296(VAL)/CG1	3.44
	296(VAL)/N	3.20
	296(VAL)/CA	3.80
	296(VAL)/CB	3.33
N3	409(PHE)/CB	3.67
	409(PHE)/CG	3.92
	295(ASP)/OD1	2.66
	409(PHE)/CD2	3.44
	295(ASP)/CG	3.89
H1	409(PHE)/CB	3.99
	295(ASP)/OD1	1.74
	409(PHE)/CD2	3.56
	295(ASP)/CB	3.93
	295(ASP)/CG	2.98
	295(ASP)/OD2	3.80
H2	409(PHE)/CB	2.94

	409(PHE)/CG	3.50
	295(ASP)/OD1	3.24
	409(PHE)/CD2	3.38
C7	461(HIS)/NE2	3.43
O1	461(HIS)/CE1	3.23
	461(HIS)/CD2	3.80
	461(HIS)/NE2	2.89
	409(PHE)/CE2	3.70
	409(PHE)/CD2	3.79
O2	465(TYR)/CE2	3.89
	465(TYR)/CZ	3.96
	465(TYR)/OH	3.10
	461(HIS)/CD2	3.64
	461(HIS)/NE2	3.52
C8	456(HIS)/CD2	3.90
	465(TYR)/CE2	3.86
	465(TYR)/CZ	3.89
	465(TYR)/OH	3.13
	456(HIS)/NE2	3.97
C9	465(TYR)/OH	3.25
	456(HIS)/CE1	3.89
	456(HIS)/NE2	3.59
	460(ASN)/C	3.80
	460(ASN)/O	3.80
	461(HIS)/N	3.98
O3	406(LEU)/O	3.94
	295(ASP)/OD1	3.95
C10	409(PHE)/N	3.73
	409(PHE)/CB	3.58
	406(LEU)/O	3.58
O4	407(MET)/C	3.53
	408(ARG)/N	2.82
	408(ARG)/CA	3.68
	408(ARG)/C	3.78
	409(PHE)/N	3.11
	409(PHE)/CB	3.80
	406(LEU)/C	3.69
	406(LEU)/O	2.66
	407(MET)/CA	3.44
N4	409(PHE)/CB	3.45
	295(ASP)/OD1	3.06
	295(ASP)/CG	3.88
H3	409(PHE)/CB	3.79
	295(ASP)/OD1	2.12 ***
	295(ASP)/CG	3.06
	295(ASP)/OD2	3.60
C11	409(PHE)/CB	3.55

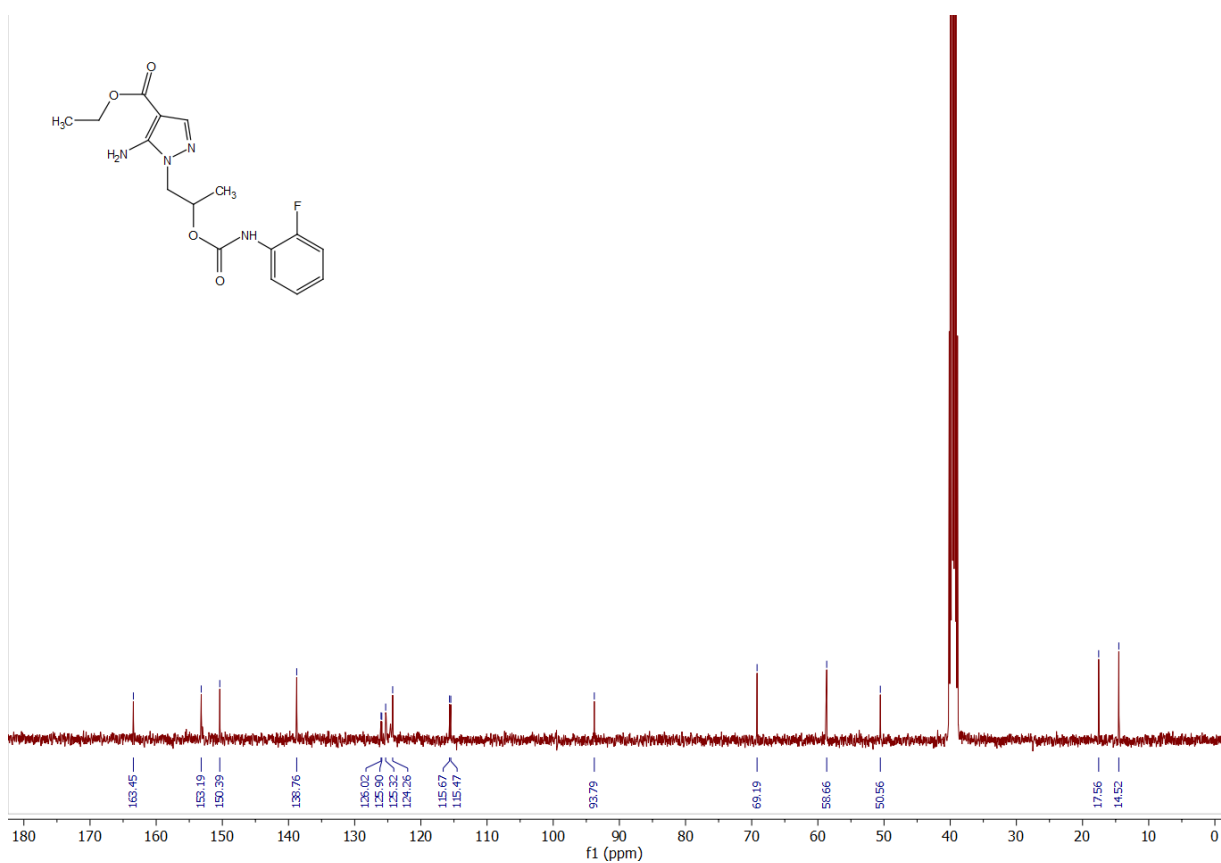
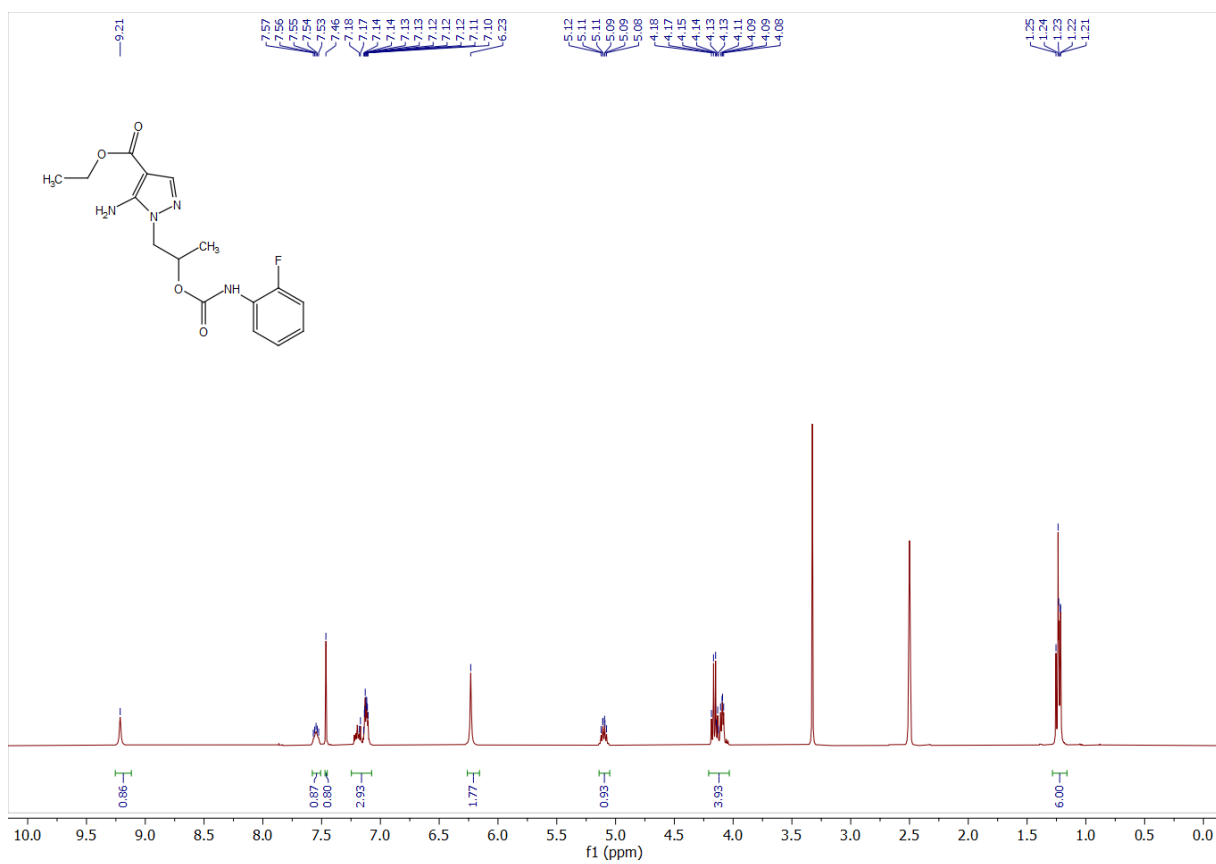
	295(ASP)/OD1	3.69
	409(PHE)/O	3.38
C12	409(PHE)/CB	3.76
	295(ASP)/OD1	3.63
	295(ASP)/OD2	3.81
	409(PHE)/O	3.11
C13	409(PHE)/O	2.89
C14	409(PHE)/O	2.98
C15	409(PHE)/O	3.25
	407(MET)/CG	3.90
C16	409(PHE)/N	3.91
	407(MET)/CA	3.88
	409(PHE)/O	3.43
C17	418(ASN)/ND2	3.97
	409(PHE)/O	3.58
	418(ASN)/OD1	3.98
F2	418(ASN)/ND2	2.93
	409(PHE)/O	3.90
	418(ASN)/CG	3.44
	418(ASN)/OD1	3.65
F3	418(ASN)/ND2	3.74
	409(PHE)/O	3.55
	418(ASN)/CG	3.63
	418(ASN)/OD1	3.07

**Figure S1.** Dose response curve of compounds **1a-d** on USP-7 enzyme obtained through GraphPad Prism 7, were reported. Each data point is the average of three separate experiments.





**Figure S2.**  $^1\text{H}$  (400 MHz,  $\text{DMSO-d}_6$ ) spectrum of compound **1a**.



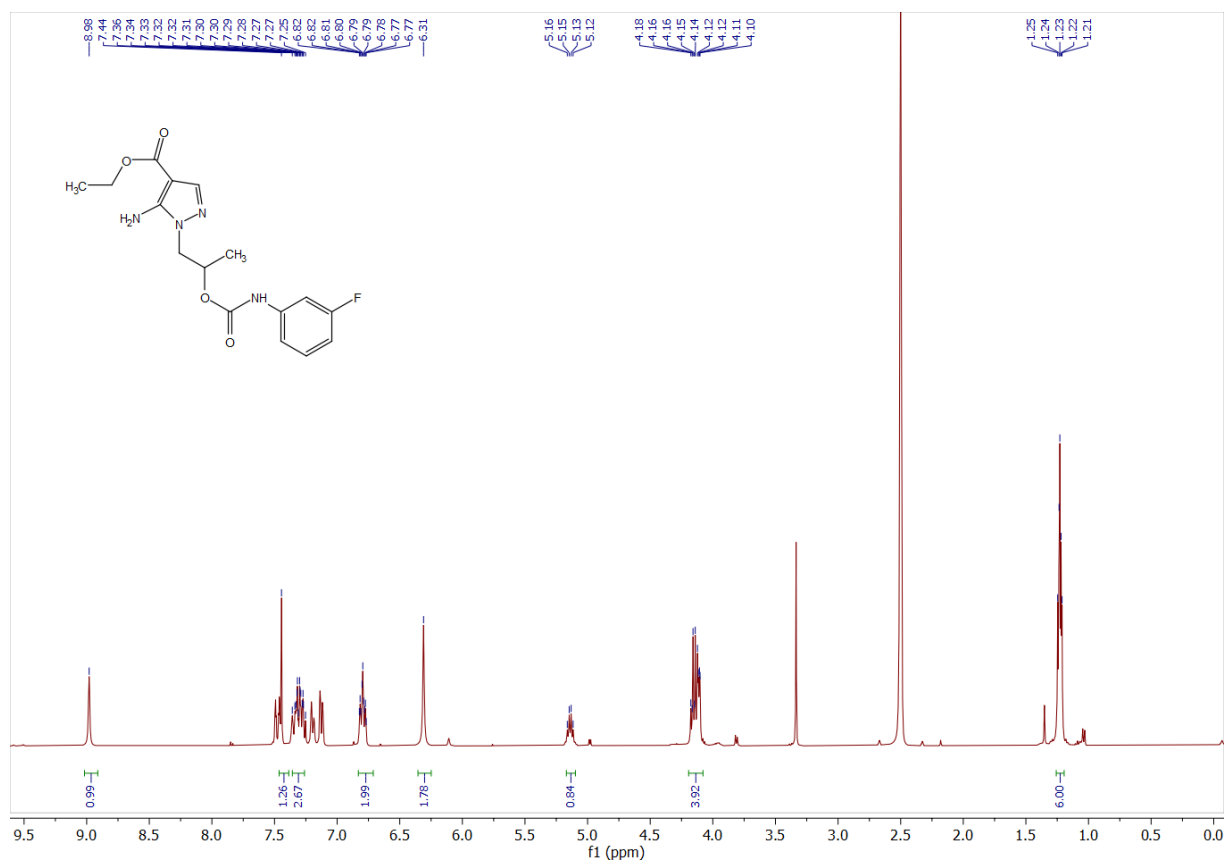


Figure S5.  $^{13}\text{C}$  (101 MHz,  $\text{DMSO-d}_6$ ) spectrum of compound 1b.

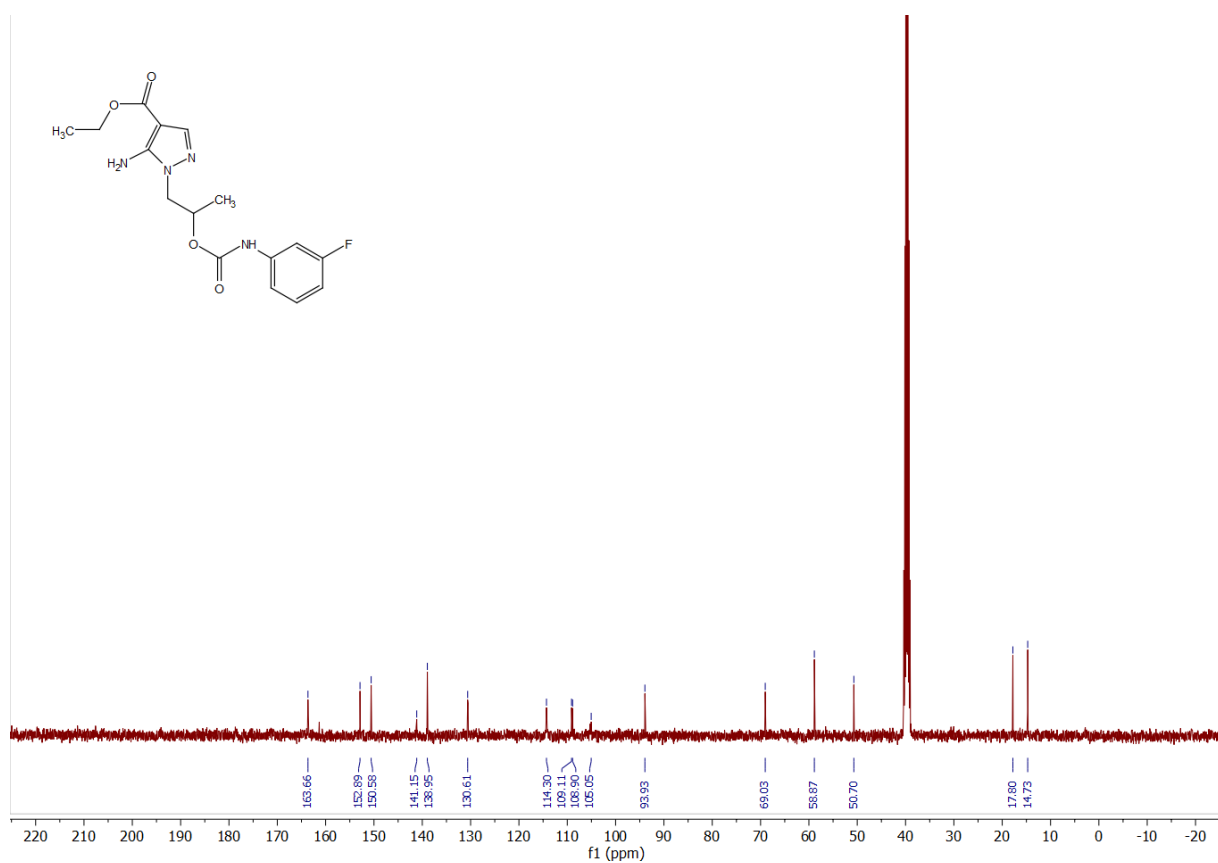


Figure S6.  $^1\text{H}$  (400 MHz,  $\text{DMSO-d}_6$ ) spectrum of compound 1c.

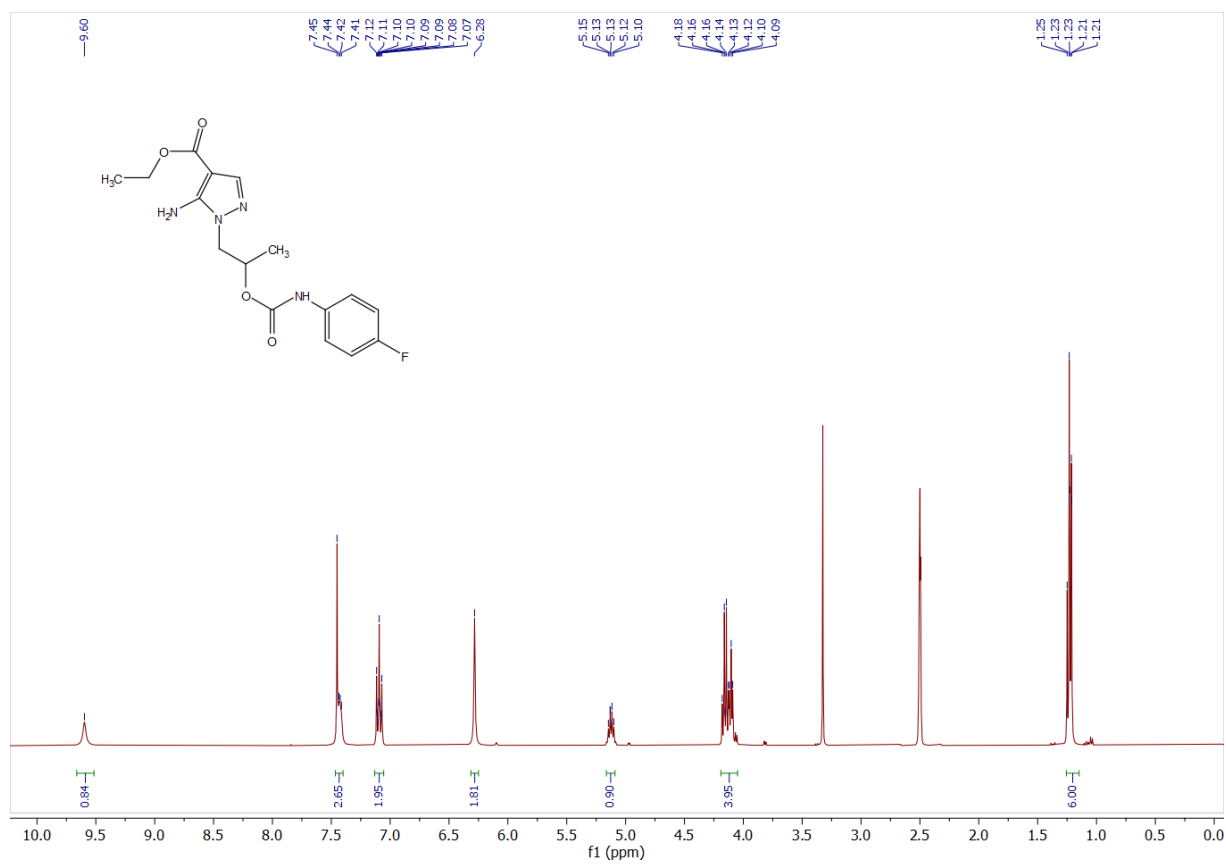


Figure S7. <sup>13</sup>C (101 MHz, DMSO-d<sub>6</sub>) spectrum of compound 1c.

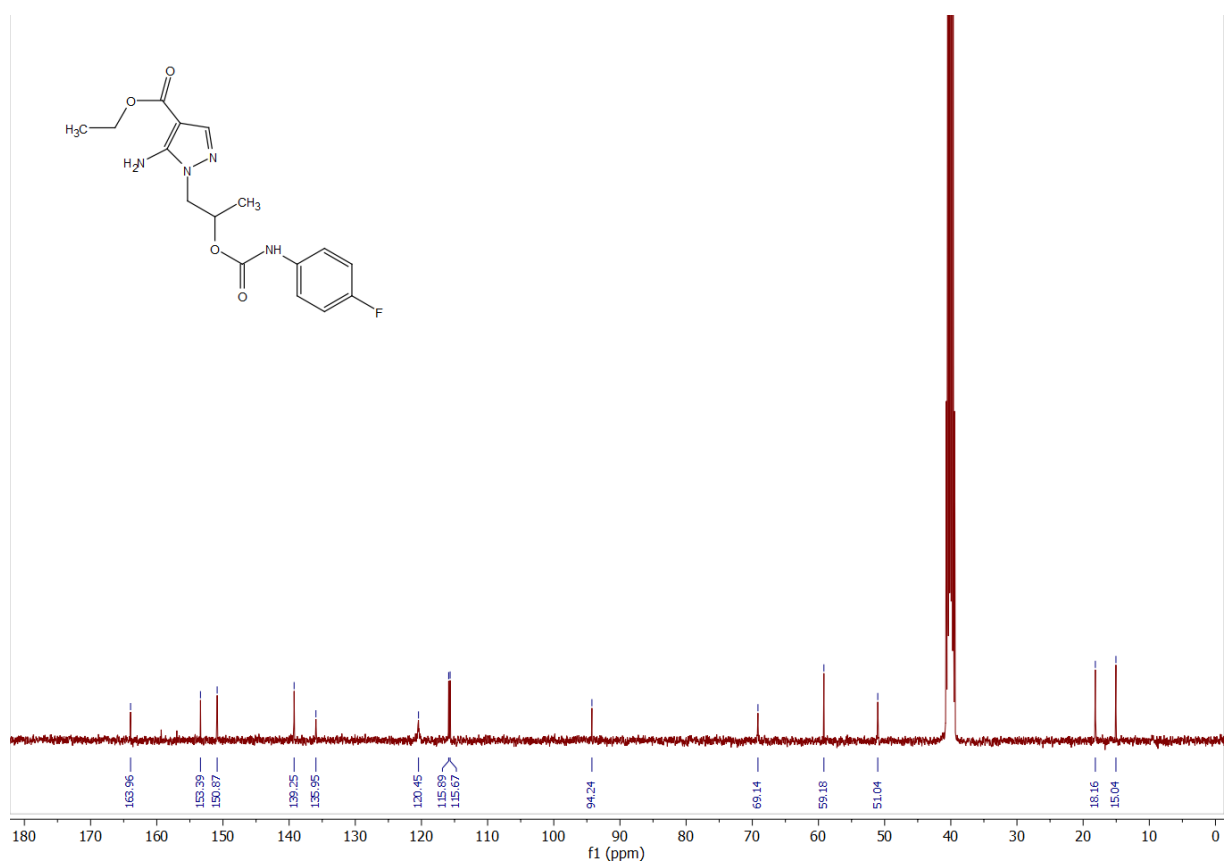


Figure S8. <sup>1</sup>H (400 MHz, DMSO-d<sub>6</sub>) spectrum of compound 1d.

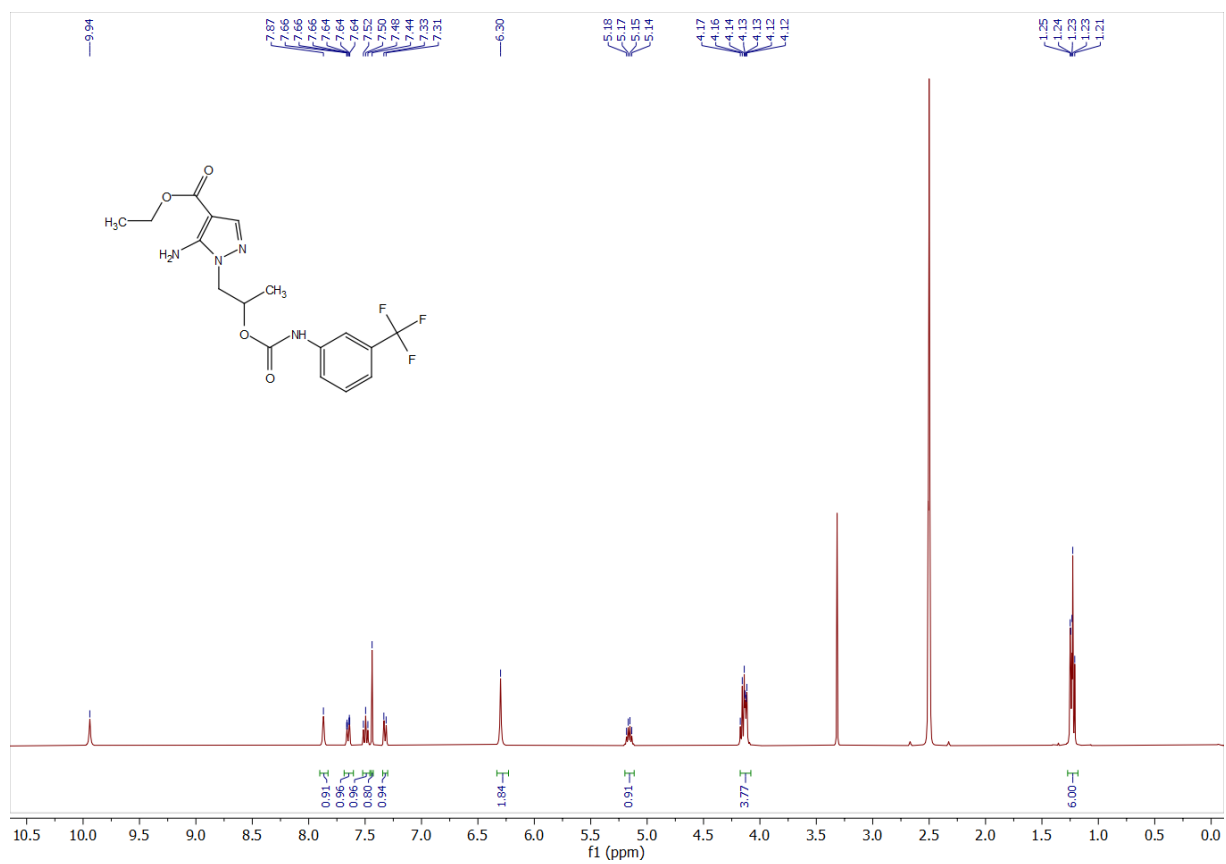


Figure S9.  $^{13}\text{C}$  (101 MHz,  $\text{DMSO-d}_6$ ) spectrum of compound 1d.

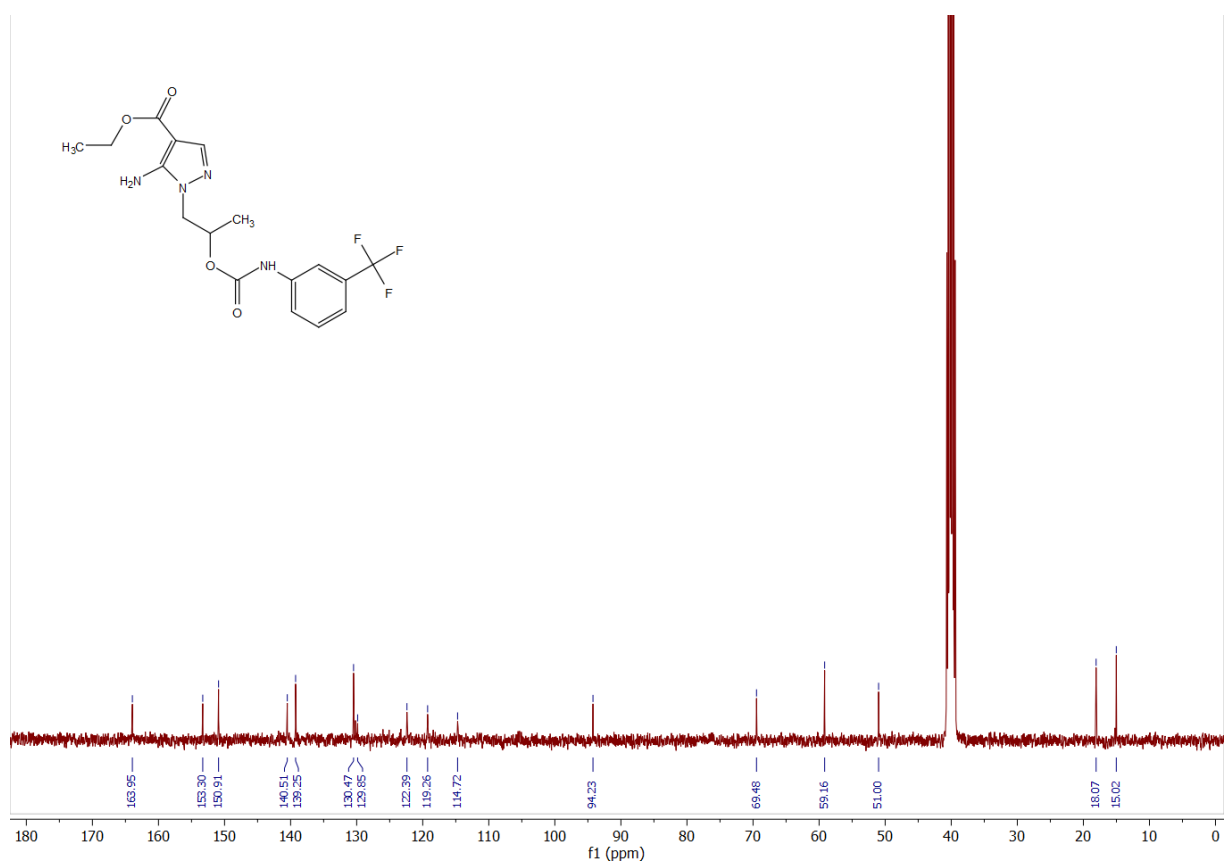


Figure S10.  $^{13}\text{C}$  (101 MHz,  $\text{DMSO-d}_6$ ) spectrum of compound 2a.

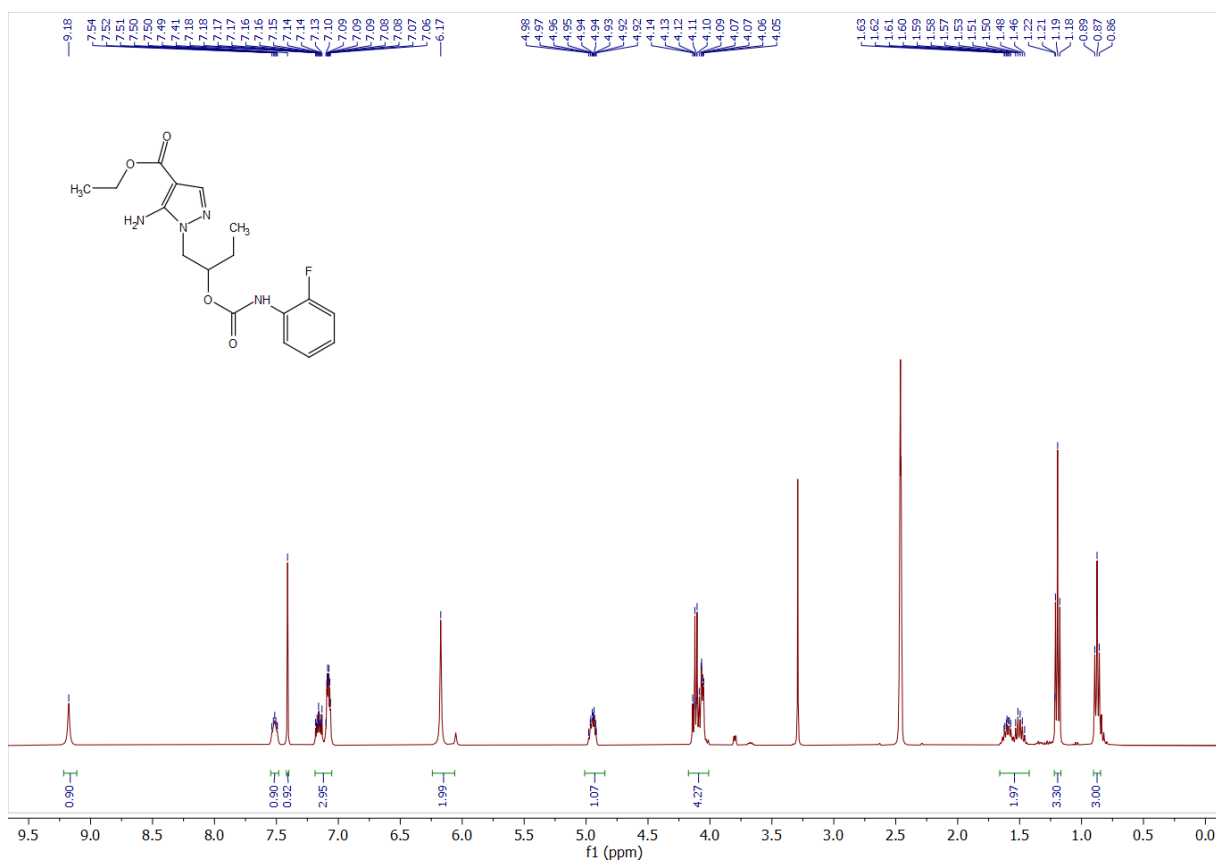


Figure S11. <sup>13</sup>C (101 MHz, DMSO-d<sub>6</sub>) spectrum of compound 2a.

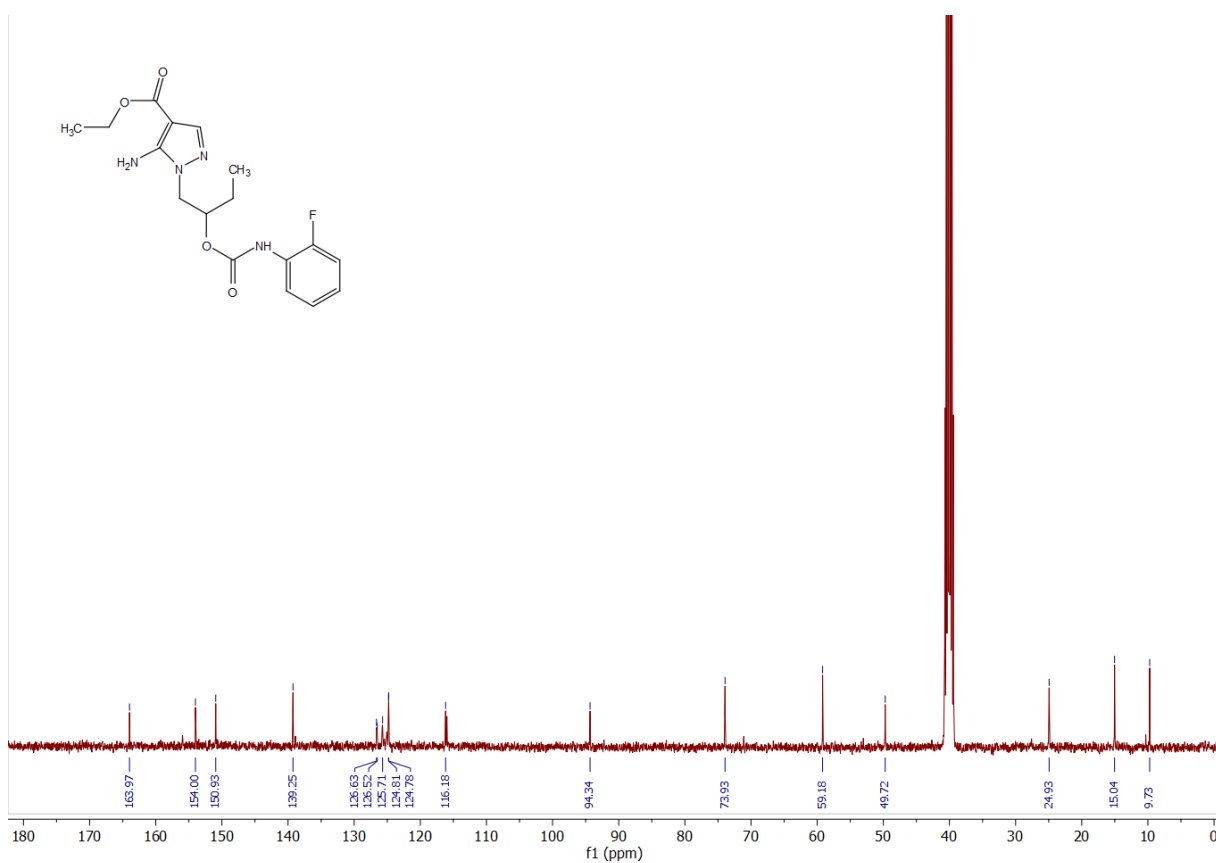


Figure S12. <sup>1</sup>H (400 MHz, DMSO-d<sub>6</sub>) spectrum of compound 2b.

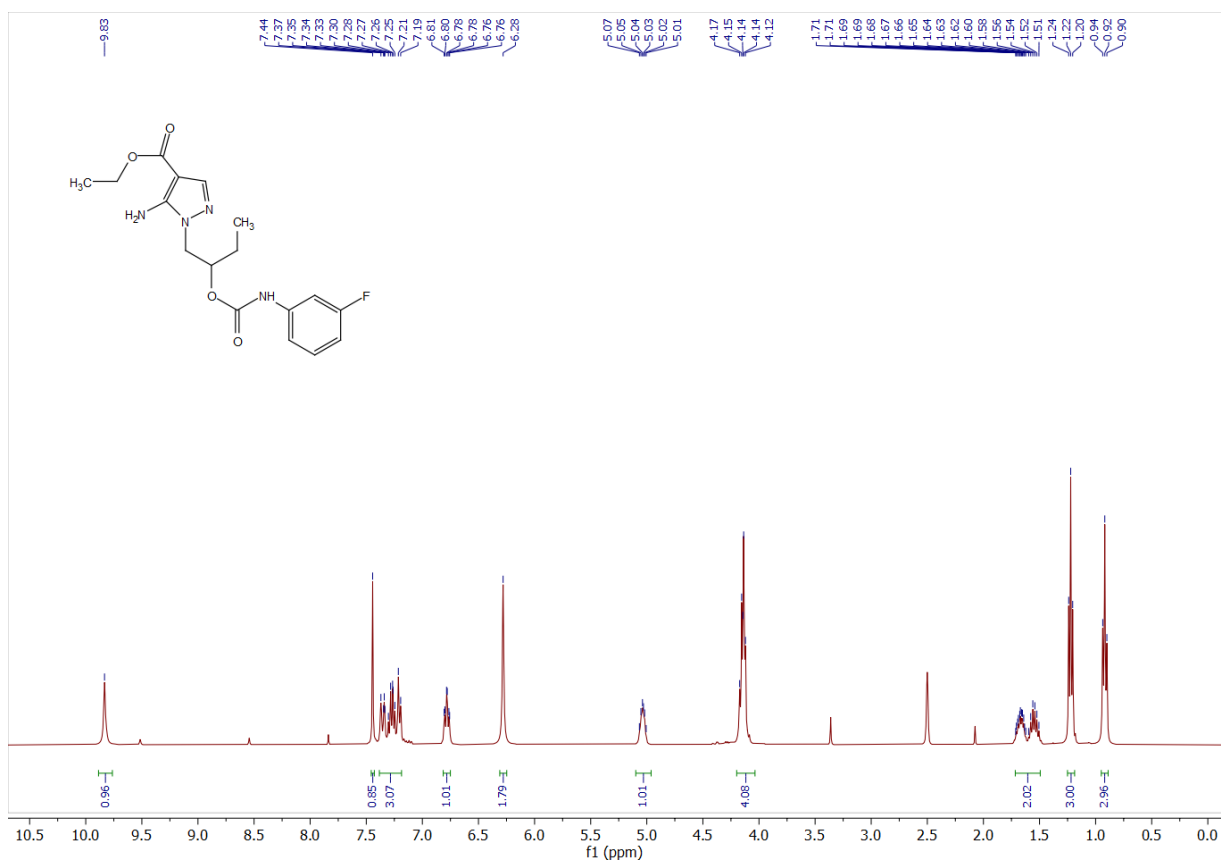


Figure S13. <sup>13</sup>C (101 MHz, DMSO-d<sub>6</sub>) spectrum of compound 2b.

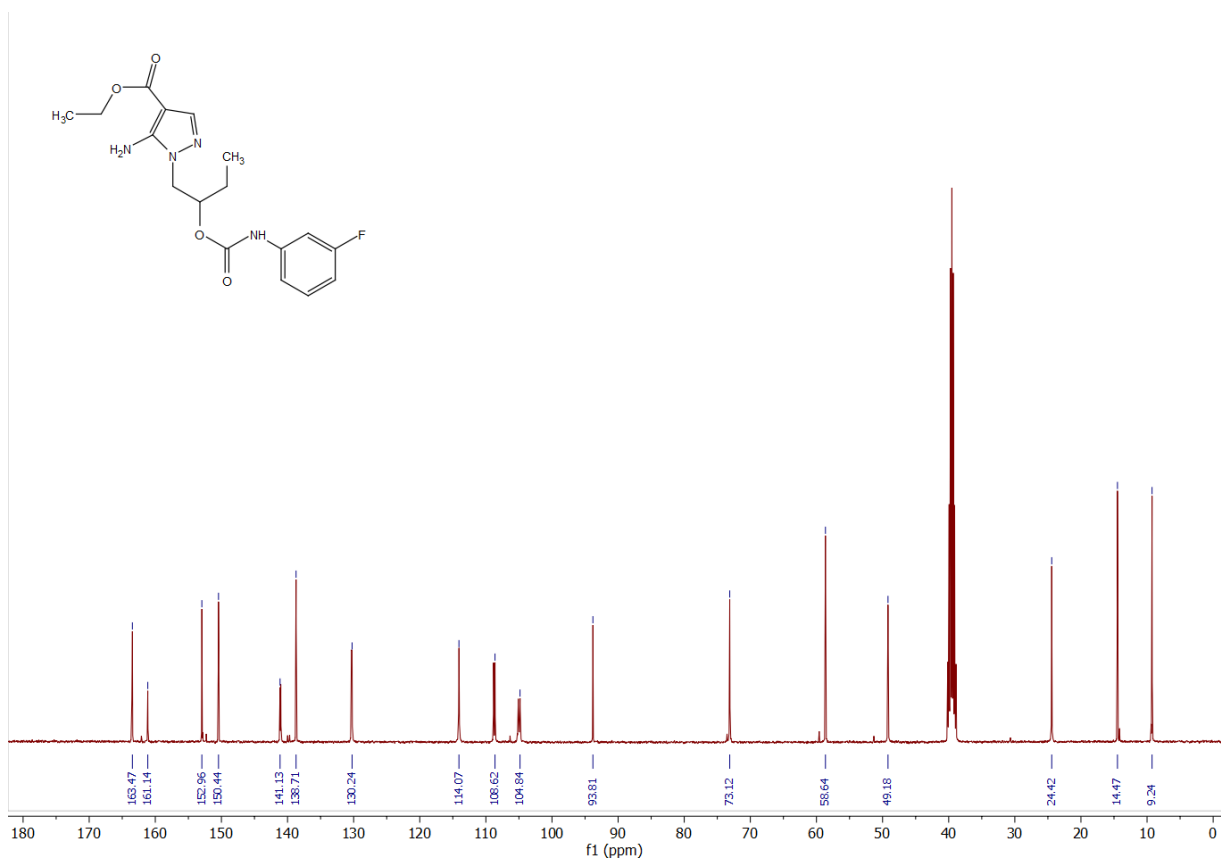


Figure S14. <sup>1</sup>H (400 MHz, DMSO-d<sub>6</sub>) spectrum of compound 2c.

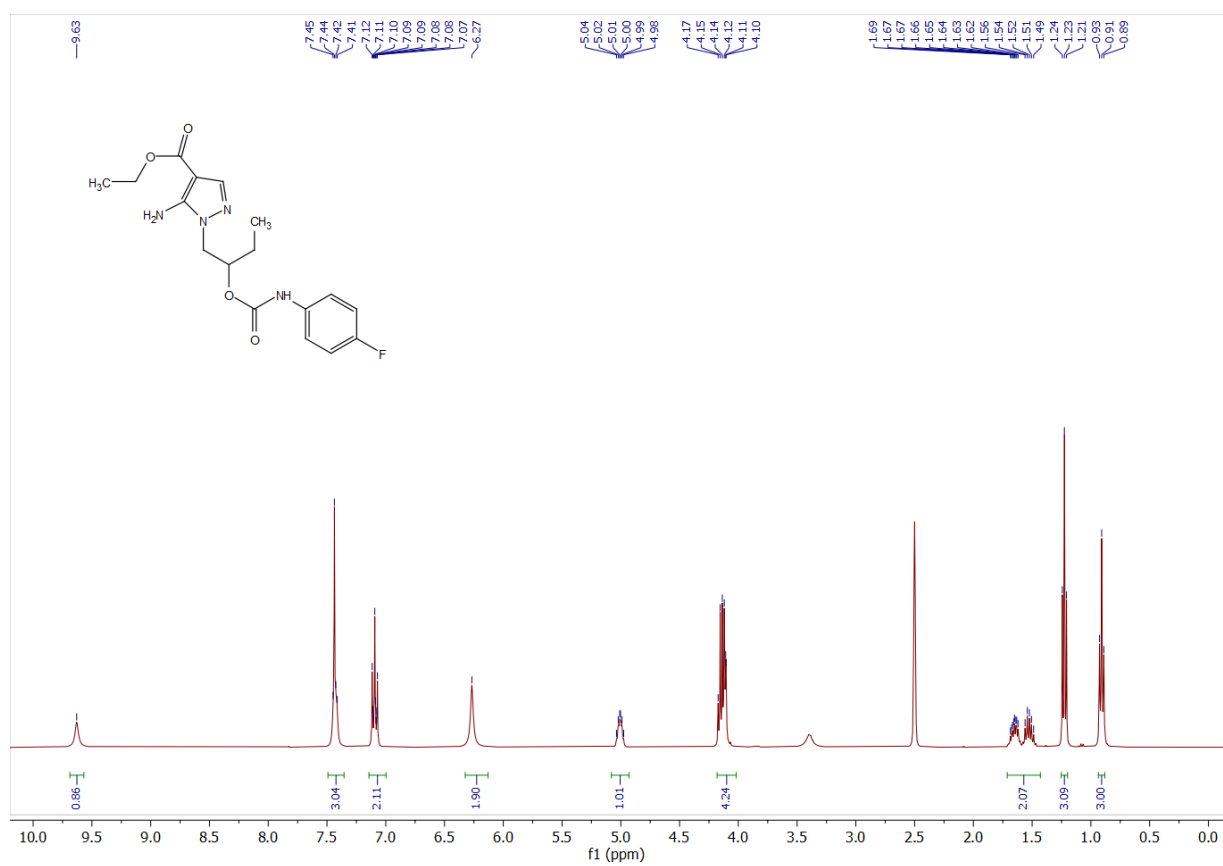


Figure S15.  $^{13}\text{C}$  (101 MHz,  $\text{DMSO-d}_6$ ) spectrum of compound 2c.

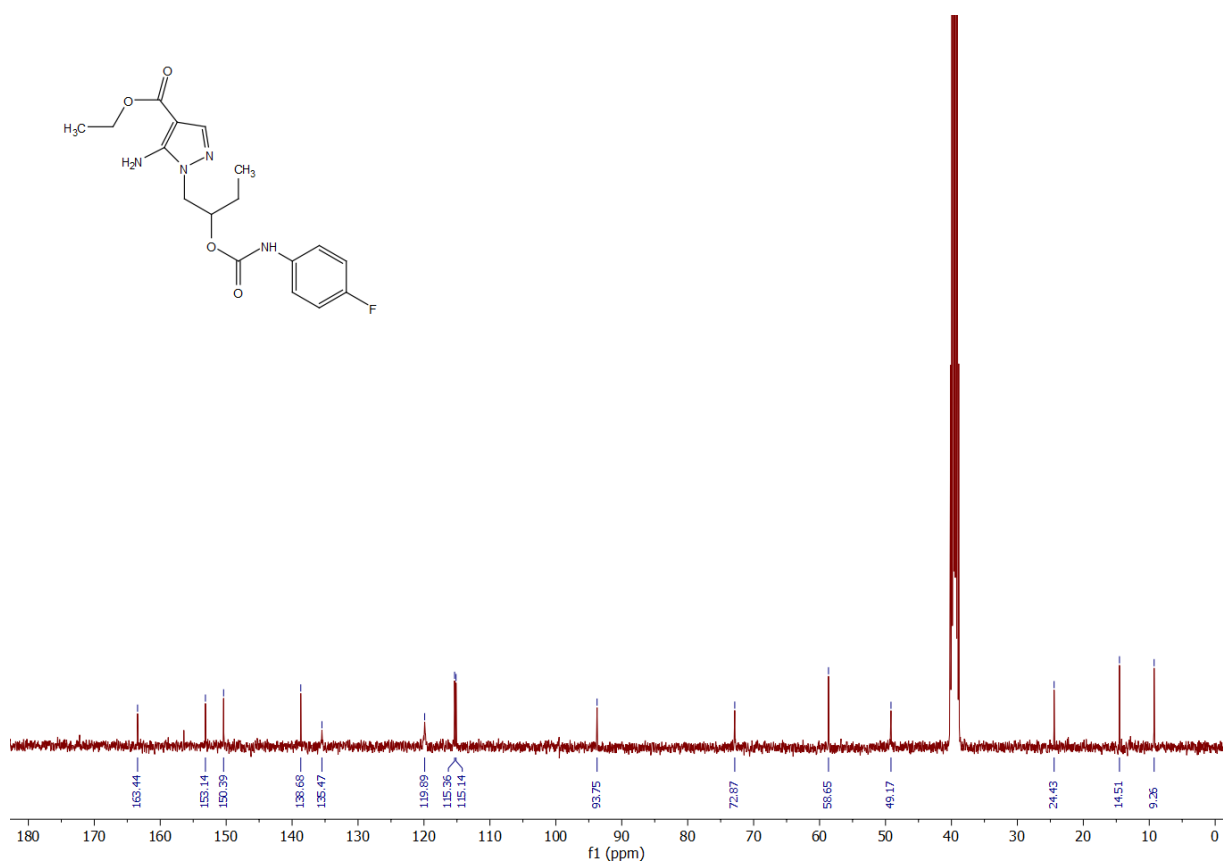


Figure S16.  $^1\text{H}$  (400 MHz,  $\text{DMSO-d}_6$ ) spectrum of compound 2d.

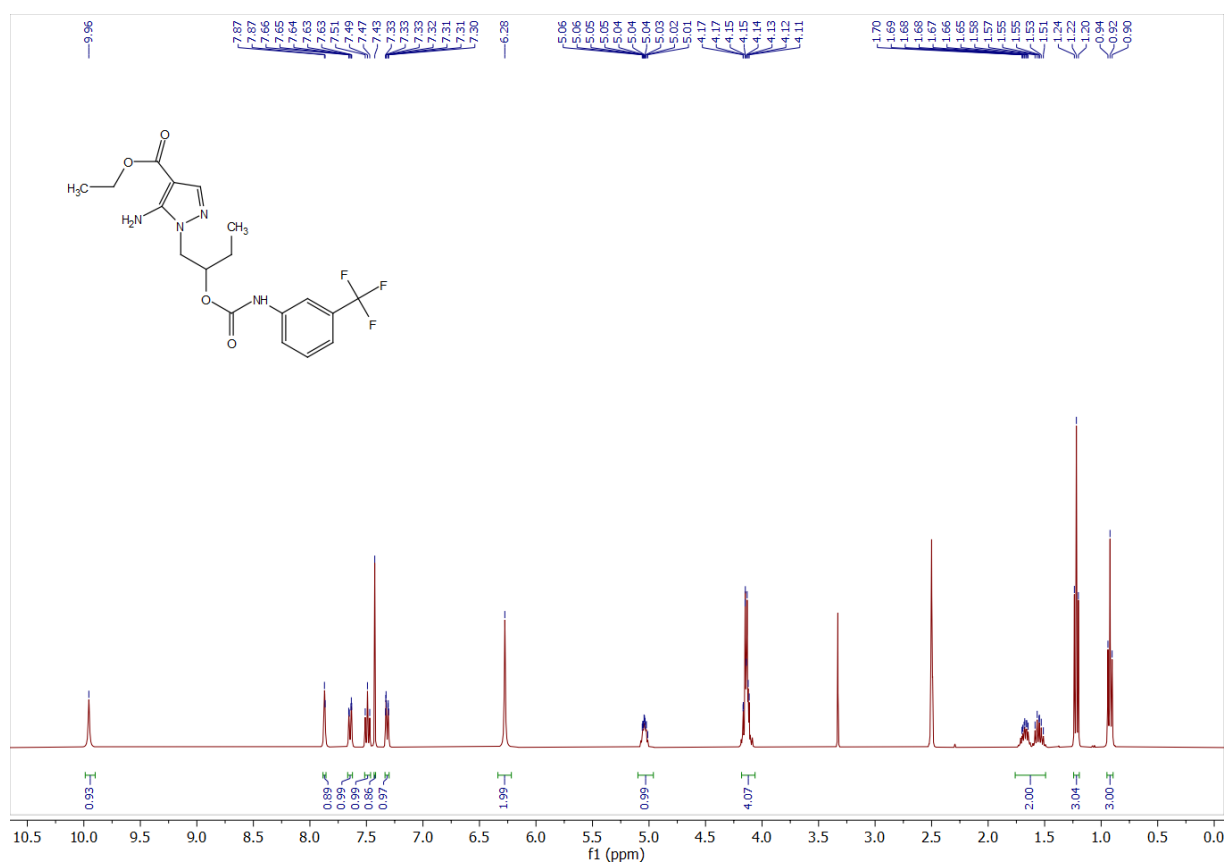


Figure S17. <sup>13</sup>C (101 MHz, DMSO-d<sub>6</sub>) spectrum of compound 2d

